CO_2 and summer insolation as drivers for the Mid-Pleistocene transition

Meike D. W. Scherrenberg[1], Constantijn J. Berends[1], Roderik S.W. van de Wal[1,2]

[1]Institute for Marine and Atmospheric research Utrecht, Utrecht University, Utrecht, the Netherlands

[2]Faculty of Geosciences, Department of Physical Geography, Utrecht University, Utrecht, the Netherlands

Correspondence to: M.D.W. Scherrenberg (M.D.W.Scherrenberg@uu.nl)

During the Mid-Pleistocene transition (MPT; ~1.2–0.8 million years ago) the dominant periodicity of glacial cycles increased from 41 thousand years (kyr) to an average of 100 kyr, without any appreciable change in the orbital pacing. As the MPT is not a linear response to orbital forcing, it must have resulted from feedback processes in the Earth system. However, the precise mechanisms underlying the transition are still under debate.

In this study, we investigate the MPT by simulating the Northern Hemisphere ice sheet evolution over the past 1.5 million years. The transient climate forcing of the ice-sheet model was obtained using a matrix method, by interpolating between two snapshots of global climate model simulations. Changes in climate forcing are caused by variations in CO_2, insolation, as well as implicit climate–ice sheet feedbacks.

Using this method, we were able to capture glacial-interglacial ~~variability~~periodicity during the past 1.5 million years and thereby reproduce the shift from 41 kyr to 100 kyr cycles without any additional drivers. Instead, the modelled frequency change results from the prescribed CO_2 combined with orbital forcing, and ice sheet feedbacks. Early Pleistocene terminations are initiated by insolation maxima. After the MPT, low interstadial CO_2 levels ~~can~~ may compensate insolation maxima which would otherwise favour deglaciation, leading to an ~~increasing~~increased length of the glacial cycle ~~periodicity. These deglaciations~~. Terminations are also ~~prevented~~affected by ~~a relatively small~~ ice volume. If the North American ice sheet~~, which, through its location and feedback processes, can generate a relatively stable climate. Larger North American ice sheets become more~~ is small or very large, it becomes sensitive to small temperature increases. A medium sized ice sheet is less sensitive through its location and the merger of the Laurentide and Cordilleran ice sheets. Therefore, Late Pleistocene terminations are also facilitated by the large ice-sheet volume, were small changes in temperature lead to self-sustained melt ~~instead~~.

~~This concept is confirmed b~~Additionally, we ~~y~~carried out experiments ~~using~~with constant ~~insolation or~~ CO_2~~. The constant CO_2 experiments generally~~ , where we can capture ~~only~~ the ~~Early Pleistocene~~41-kyr cycles and~~, while those with constant insolation only capture~~ some Late Pleistocene cycles. ~~Additionally, we find that a lowering of~~ However, no persistent 100-kyr periodicity is established. Experiments with constant (or evolving) CO_2 concentrations ~~leads to an increasing number~~

~~of~~did not generate a substantial precession signal in the ice volume. Instead, the frequency is dominated by successful terminations, which are initiated by strong (generally obliquity) insolation maxima~~ that fail to initiate terminations. These~~.

Our results therefore ~~suggest a regime shift, where during the Early Pleistocene,~~indicate that the glacial cycle periodicity of the past 1.5 million years can be described by changes in insolation, CO_2 and ice sheets feedback processes, and that maintaining low CO_2 throughout insolation maxima may prolong glacial cycles~~ are dominated by orbital oscillations, while Late Pleistocene cycles tend to be more dominated by CO_2. This implies that the MPT can be explained by a decrease in glacial CO_2 concentration superimposed on orbital forcing~~.

1. Introduction

During the ~~Mid-Pleistocene transition (~~MPT~~; ~1.2 – 0.8 million years ago)~~, the duration of glacial cycles shifted from 41 kyr to an average of 100 kyr, but the main mechanisms behind this change are still under debate. Glacial cycles are paced by orbital cycles, namely precession (~19/23 kyr), obliquity (~41 kyr), and eccentricity (~98/400 kyr), which determine the latitudinal and seasonal distribution of solar radiation received by the Earth. Ice sheets are especially sensitive to summer insolation, as regions may undergo melt and a small change in temperature or insolation can strongly alter melt rates. As a result, the 41 kyr periodicity during the Early Pleistocene (2580 – 800 kyr ago) mostly follows the obliquity cycle (e.g., Huybers and Tziperman, 2008; Tabor et al., 2015; Watanabe et al., 2023), but the mechanisms behind the average 100 kyr periodicity of the Late Pleistocene (800 – 11 kyr ago) are more difficult to explain. It has been suggested that the 100 kyr periodicity is a non-linear response to predominantly obliquity (e.g., Huybers and Wunsch, 2005), precession and eccentricity (e.g., Lisiecki, 2010; Hobart, et al. 2023; Blackburn et al., 2024), or a combination of orbital cycles (e.g., Huybers, 2011; Feng and Bailer-Jones, 2015; Tzedakis, et al. 2017). Nevertheless, the transition from 41 kyr to 100 kyr glacial cycles took place without any considerable change in the orbital cycles, and ~~it must~~ therefore ~~have resulted from~~ feedback processes within the Earth's system must have contributed to the MPT.

One overarching hypothesis ~~for~~that could partially explain the MPT ~~suggest that the~~concerns ice~~ sheets display a~~ sheet threshold ~~regime~~regimes (see Berends, et al. 2021a; Paillard, 1998~~).~~): Small or flat ice sheets can easily melt at insolation maxima. Medium-sized ice sheets may survive insolation maxima due to albedo and topography feedbacks, facilitating low temperatures in glaciated regions. Large ice sheets become vulnerable through positive feedbacks such as the elevation-temperature feedback, albedo feedbacks, and high basal temperatures enhancing sliding (Bintanja and van de Wal, 2008), and Proglacial Ice Sheet Instability (PLISI; see ~~Hinck et al., 2022;~~ Quiquet et al., 2021; Hinck et al., 2022; Scherrenberg et al., 2024). This is further supported by several studies showing that the Late Pleistocene glacial cycles only melt once they reach a certain ice volume (Parrenin and Paillard, 2003; Bintanja and van de Wal, 2008; Abe-Ouchi et al., 2013; ~~Parrenin and Paillard, 2003; Bintanja and van de Wal, 2008; Berends et al., 2021a).~~Verbitsky et al., 2018; Berends et al., 2021a). These threshold regimes can therefore act as a precondition that facilitates the MPT, but require another process (e.g., long term cooling) to prompt a shift in the ice volume rhythm.

~~Alternatively, it~~It has also been suggested that the MPT is caused by regolith removal, as first proposed by Clark and Pollard (1998). The regolith hypothesis states that sediments covered North America during the Early Pleistocene. Sediments are easily deformed and enhance sliding, creating flatter ice sheets with relatively larger ablation areas. ~~Ice~~Therefore, if ice sheets are superimposed on sediments, they are ~~therefore~~ more vulnerable to small changes in forcing. Once this sediment was removed by the erosive action of the ice sheet, friction increased, reducing ice sheet flow. This produces thicker ice sheets that may survive insolation maxima. Several modelling studies were dedicated to this regolith hypothesis and were able to capture characteristics of the MPT (e.g., Tabor and Poulsen 2016, Ganopolski and Calov, 2011; Mitsui et al., 2023). Recently, Willeit et al. (2019) used a coupled climate-ice-sheet-carbon-cycle model and was able to reproduce the MPT using prescribed gradual atmospheric CO_2 decrease and regolith removal. The regolith theory is also supported by geological data which show a change in the composition of glacial sediments (e.g., Roy et al., 2004; Portier et al., 2021).

Alternative explanations argue that the carbon cycle ~~instead~~ plays a major role in controlling the transition from 41 kyr to 100 kyr glacial cycles. During the Late Pleistocene glacial cycles, glacial-interglacial variations in CO_2 were roughly 90 ppm. (Bereiter et al., 2015). This variation in CO_2 can be largely attributed to the ocean (e.g., Sigman and Boyle, 2000; Brovkin et al., 2012). During glacial periods, CO_2 solubility increases due to lower ocean temperatures, which is further enhanced by increased alkalinity (Kurahashi-Nakamura et al., 2010; Sigman et al., 2010). Glacial-erosional and enhanced dust concentrations in the atmosphere provides nutrients to the Southern Ocean. This increases the biological productivity (Martin, 1990; Martínez-García et al. 2014; Chalk et al., 2017; Saini et al., 2023) and eventually leads to more uptake of CO_2 in the deep-ocean. Additionally, decreased deep-ocean ventilation during glacial periods may have more efficiently trapped carbon (Hasenfratz et al., 2019), which could be explained by increased sea ice extent (Menviel, 2019), or enhanced ocean stratification (Bouttes et al., 2009; Adkins, 2013; Qin et al., 2022). These processes in the carbon cycle are important for decreasing CO_2 levels in the atmosphere during Late Pleistocene glacial periods, but perhaps they also played a crucial role during the MPT. After the MPT, glacial CO_2 concentrations may have dropped due to increased deep-ocean carbon storage (Köhler and Bintanja, 2008; Lear et al., 2016; Farmer et al., 2019; Qin et al., 2022; Thomas et al., 2022~~; Qin et al., 2022~~) which could, for example, have resulted from increased Antarctic bottom water formation due to a change in circulation (e.g., Pena et al., 2014), or an increase in sea ice extent (Detlef et al., 2018).

Nevertheless, despite the complexity and uncertainties in the carbon cycle, atmospheric CO_2 can be measured from ice cores (e.g. Bereiter et al. 2015), or estimated through proxies (e.g. Hönisch et al., 2009; Da et al., 2019; Dyez et al., 2018; Yamamoto et al., 2022). Ice core CO_2 records tend to have low uncertainties ~~but~~, as CO_2 can be measured directly from bubbles or clathrates in the ice, which contain a snapshot of the paleo-atmosphere. However, the current oldest continuous record dates back to only 800 kyr ago (Bereiter et al., 2015~~),~~) which does not capture the MPT. ~~Other~~CO_2 can also be estimated indirectly from certain isotope ratios (e.g. boron isotopes; see Hönisch et al., 2009; Dyez et al., 2018; Da et al., 2019; or leaf-wax; Yamamoto et al., 2022), allowing for CO_2 records ~~can provide us information by indirectly measuring signals controlled by~~

~~CO_2 variations, though at the expense of~~ that extent beyond the ice-records. However, to generate a CO_2 record from a proxy requires physical and chemical assumptions, which results in a higher uncertainty. ~~For example, recently~~Recently, Yamamoto et al. (2022) published a ~~continuous 1.5 million year CO_2 record~~ reconstruction based on a leaf-wax indicator, which was calibrated to the 800 kyr ice core record. The record by Yamamoto et al. (2022) is currently the only continuous CO_2 proxy that dates back to almost 1.5 million years ago, and thus provides a new opportunity for modelling studies on the MPT.

In this study, we simulate the past 1.5 million years using an ice-sheet model without any change in model set-up over time, and a constant sediment mask. Our main goal is to explore if we can simulate the frequency change during the MPT, and the possible mechanisms behind it, based on only prescribed CO_2 and insolation variations. The purpose is therefore not to make perfect spatial reconstructions, but rather to explain the frequency change of glacial-interglacial variability. To provide the model with information on climate, we use a matrix method which is based on interpolated 2D-time-slices from general circulation models (GCM). The temporal climate interpolation is driven by prescribed CO_2 and insolation (see Berends et al., 2018; Scherrenberg et al., 2024). Here we use the CO_2 levels from Yamamoto et al. (2022), which ~~yields~~ enables us~~us the opportunity~~ to prescribe reconstructed CO_2 concentrations during the MPT. This method allows us to provide transient climate forcing at a significantly reduced computational time compared to GCM's or intermediate complexity models (e.g., Ganopolski and Calov, 2011; Willeit et al., 2019). Temperature change is mainly driven by prescribed CO_2 records from leaf-wax proxy (1450-0 kyr ago) ~~or ice cores (800-0 kyr ago),~~ combined with caloric summer half-year insolation (Tzedakis et al. 2017). To establish the ~~effect~~importance of CO_2 and insolation variations on glacial-interglacial time-scales, we run the same 1450 kyr experiments with constant CO_2 or insolation levels.

2. Methods

To simulate ice-sheet evolution during the past 1.5 million years, we use the vertically integrated ice-sheet model IMAU-ICE version 2.1 (Berends et al., 2022). North America, Eurasia and Greenland are simulated in separate model domains, which are shown in Fig. 1.

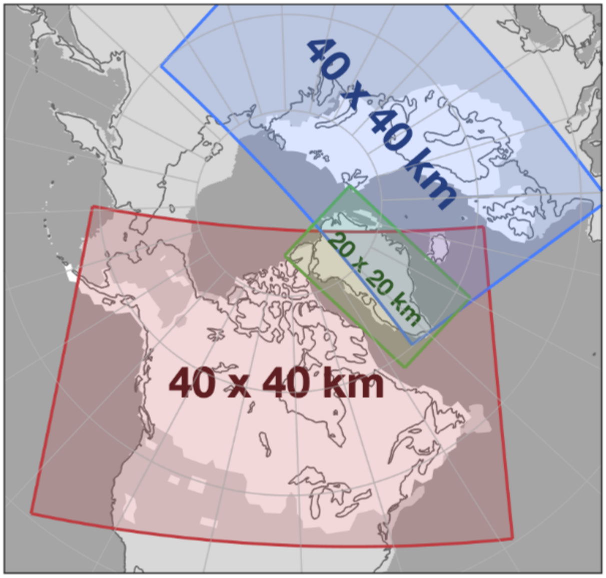

Figure 1. The extent and resolution of the ice-sheet model domains: North America (red), Greenland (green) and Eurasia (blue). For reference, the ICE-6G LGM ice sheet of Peltier et al. (2015) is shown in white. Ice in overlapping regions is removed (e.g., Greenland in the North American domain).

The flow of ice is calculated using the shallow ice / shallow shelf approximation (Bueler and Brown, 2009). Basal hydrology is based on Martin et al. (2011). To calculate basal friction, we apply a present-day sediment map for North America (Gowan et al., 2019), and, as this map does not cover Eurasia, we generate a friction map for this continent using the sediment thickness by Laske and Masters (1997). ~~While sediment distribution may have changed through transport and erosion, we keep a constant sediment map to test whether it is possible to capture the MPT without any changes in basal friction.~~

This friction map is static, but a simulation with a time-variable sediment mask is presented in the supplementary material. To simulate bedrock changes due to ice sheet load, we use an Elastic Lithosphere, Relaxing Asthenosphere model (Le Meur and Huybrechts, 1996). If bedrock topography is below sea level, it is considered as ocean or lake. At the grounding line we include a sub-grid friction scaling scheme based on Leguy et al. (2021) and Feldmann et al. (2014). Ice is removed if the thickness at the calving front is below 200 m. Additionally, floating ice beyond the continental shelf is always removed. To calculate basal melt, we use a depth dependent sub-shelf parameterization based on Martin et al. (2011). Ocean temperatures are based on de Boer et al. (2013), and while they evolve over time, they do not vary spatially within a model domain. For the surface mass balance (SMB), we use IMAU-ITM (insolation, temperature model), which includes a melt parameterization (Bintanja et al., 2002) that depends on temperature, albedo and insolation, a snow-rain partitioning scheme (Ohmura et al., 1999), and a refreezing scheme (Huybrechts and de Wolde, 1999). IMAU-ITM has been shown to be perform well for present-day Greenland conditions (see Fettweis et al., 2020).

2.1 Climate forcing

To calculate the transient climate forcing over the past 1.5 million years, we interpolate between GCM-calculated climates of pre-industrial (PI) and the Last Glacial Maximum (LGM). Since the choice of GCM climates can cause large differences in the modelled ice sheets (Alder and Hostetler, 2019; Niu et al., 2019; Scherrenberg et al., 2023), we use a climate ensemble obtained from the Paleoclimate Modelling Intercomparison Project (PMIP4; Kageyama et al., 2017, 2018) rather than a large quantity of time-slices from a single model. The four simulations that had all data necessary for our simulations are MIROC (Ohgaito et al., 2021), MPI (Mauritsen et al., 2019), AWI (Shi et al., 2023) and INM (Volodin et al., 2018). Differences in topography between climate and ice-sheet model are accounted for by applying a lapse rate correction for temperature, and by applying a correction for precipitation with wind-ward and leeward topography effects based on the approach by Roe and Lindzen (2001). The technical details of these methods are described in Scherrenberg et al. (2023).

To interpolate the climate time-slices through time we use a matrix method (see Berends et al., 2018; Scherrenberg et al., 2023; Scherrenberg et al., 2024). Equations governing the matrix method are described in Appendix A. Here we provide a brief, qualitative summary.

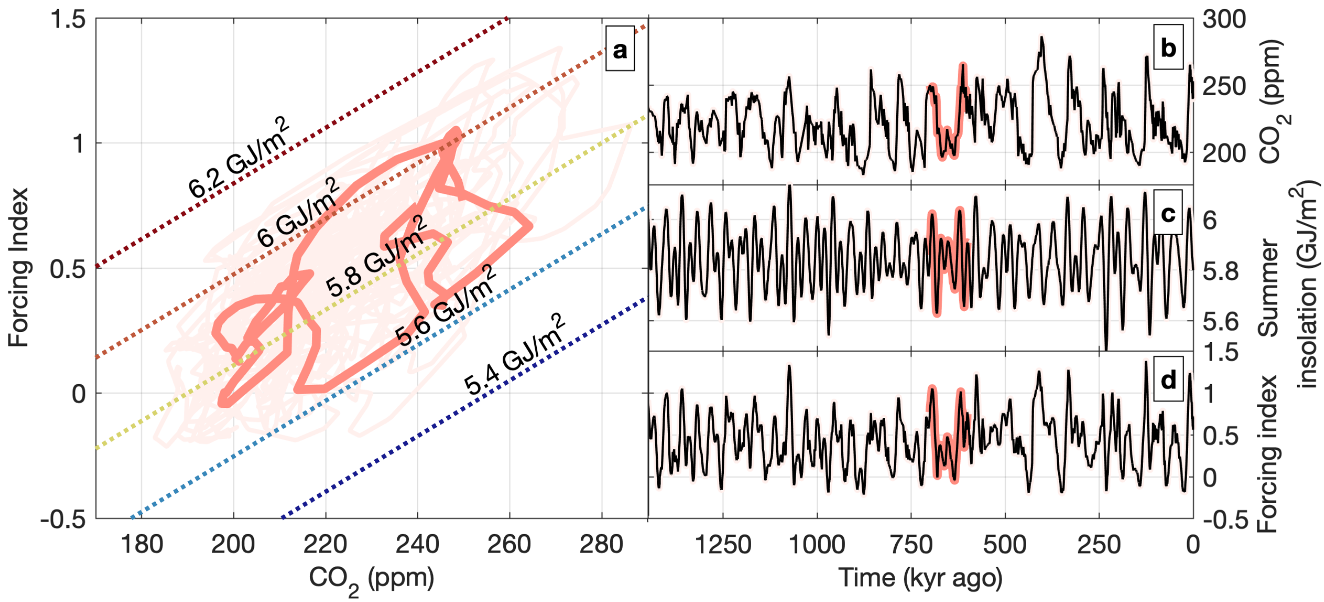

~~**Figure 2.** The forcing index (a,d) is a combination of CO_2 (b; x-axis in a) and caloric summer-half year insolation at 65°N (c; diagonal lines in a). Red shows the evolution of the forcing index over one glacial cycle, while pink (see panel a) shows the forcing index over the entire simulation.~~

Temperature depends on the prescribed external forcing (CO_2 and summer insolation) and the modelled ice-sheet, to create a first-order approximation of the ice-albedo feedback. Fig. 2 shows how the prescribed CO_2 and caloric summer insolation (Tzedakis et al. 2017) are combined to calculate the external forcing index. To approximate the albedo feedback, we follow the approach by Berends et al. (2018), where the monthly/latitudinally varying insolation is multiplied with the modelled albedo to yield the ‘absorbed insolation’. As the modelled albedo depends on the modelled ice-sheet extent and snow cover, this introduces the feedback from the ice sheet back onto the climate.

Precipitation is modelled similarly, but there the ice-sheet term relates to the (modelled, local) ice thickness rather than the extent, in order to approximate the plateau desert effect. A geometry-based correction, which includes the orographic forcing of precipitation by upslope winds (Roe and Lindzen, 2001), helps to more accurately track the higher precipitation rates at the (moving) ice margin.

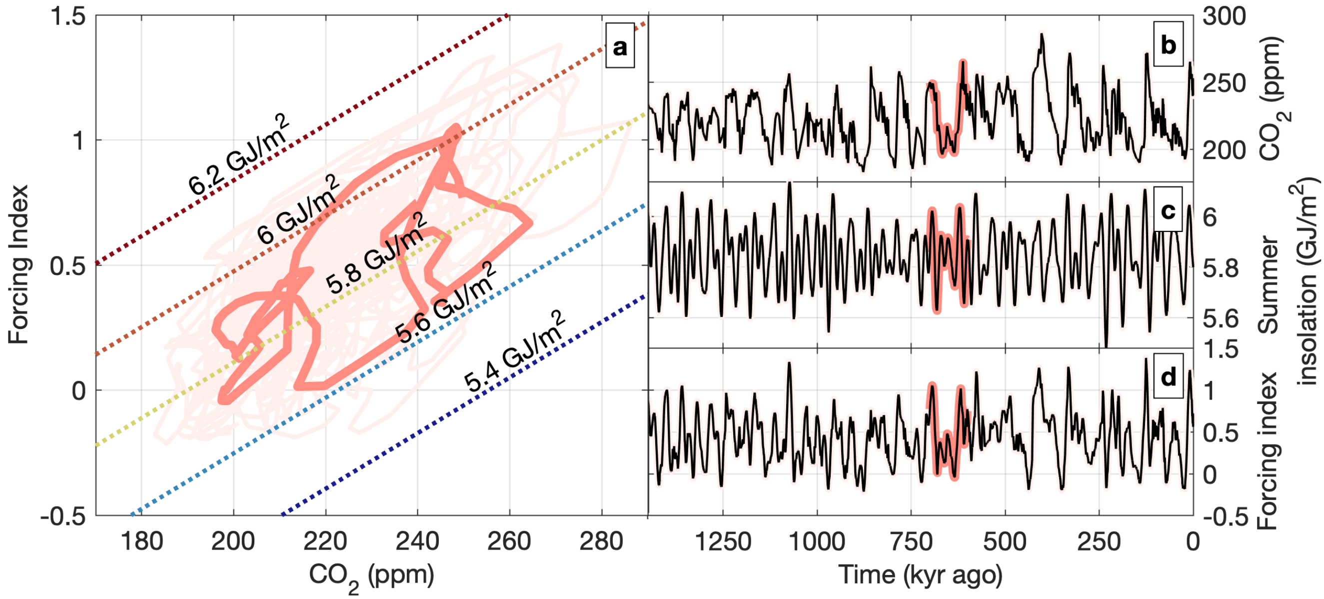

Figure 2. The forcing index (a,d) is a combination of CO_2 (b; x-axis in a) and caloric summer-half year insolation at 65°N (c; diagonal lines in a). Red shows the evolution of the forcing index over one glacial cycle, while pink (see panel a) shows the forcing index over the entire simulation.

2.2 Benthic $\delta^{18}O$

Challenges in studying the MPT are the large uncertainties in sea level reconstructions, especially during the Early Pleistocene. The benthic $\delta^{18}O$ record contains the combined signals of ice volume and deep-water temperature, which are difficult to disentangle. To validate our results, we simulate benthic $\delta^{18}O$ by modelling a separate contribution from deep-water temperature and ice volume.

IMAU-ICE includes a $\delta^{18}O$ model based on the approach by de Boer et al. (2013). This approach uses a depth-integrated advection solver to calculate the evolution of the englacial isotope content, which is forced at the surface by an elevation-dependent parameterisation following Clarke et al. (2005). The governing equations of this approach are detailed in appendix B. The benthic $\delta^{18}O$ contribution from ice volume is calculated by integrating the modelled englacial isotope content over all three modelled ice sheets.

To obtain the deep-water temperature we calculate global temperatures based on CO_2, and we apply a 3000-year running-mean to reflect the lag between the atmosphere and deep-ocean. We then linearly convert deep-water temperatures to deep-water $\delta^{18}O$ contribution.

Results

In this section, we show the results from our 1.5-million-year simulations. First, we present our baseline simulation, after which we explore the mechanisms behind the simulated MPT. In the last section we present experiments with either constant insolation or constant CO_2.

3.1 Baseline results

We conduct the 1.5-million-year baseline simulation, where temperature evolves with prescribed CO_2 from leaf-wax proxy (Yamamoto et al., 2022), caloric summer insolation (Tzedakis et al., 2017), and an albedo feedback. ~~As the leaf-wax record has higher uncertainties compared to ice-core records~~In Fig. S1, we ~~also conduct the baseline_icecore experiment~~show results from a 0.8-million-year simulation which is forced by the ice core CO_2 record from Bereiter et al. (2015) instead. ~~However, this continuous~~The results of that simulation are very close to those of the Baseline simulation, as the two CO_2 ~~record covers neither~~records are very similar (reflecting the ~~MPT nor the Early Pleistocene.~~fact that the leaf-wax based reconstruction was calibrated to the ice core record).

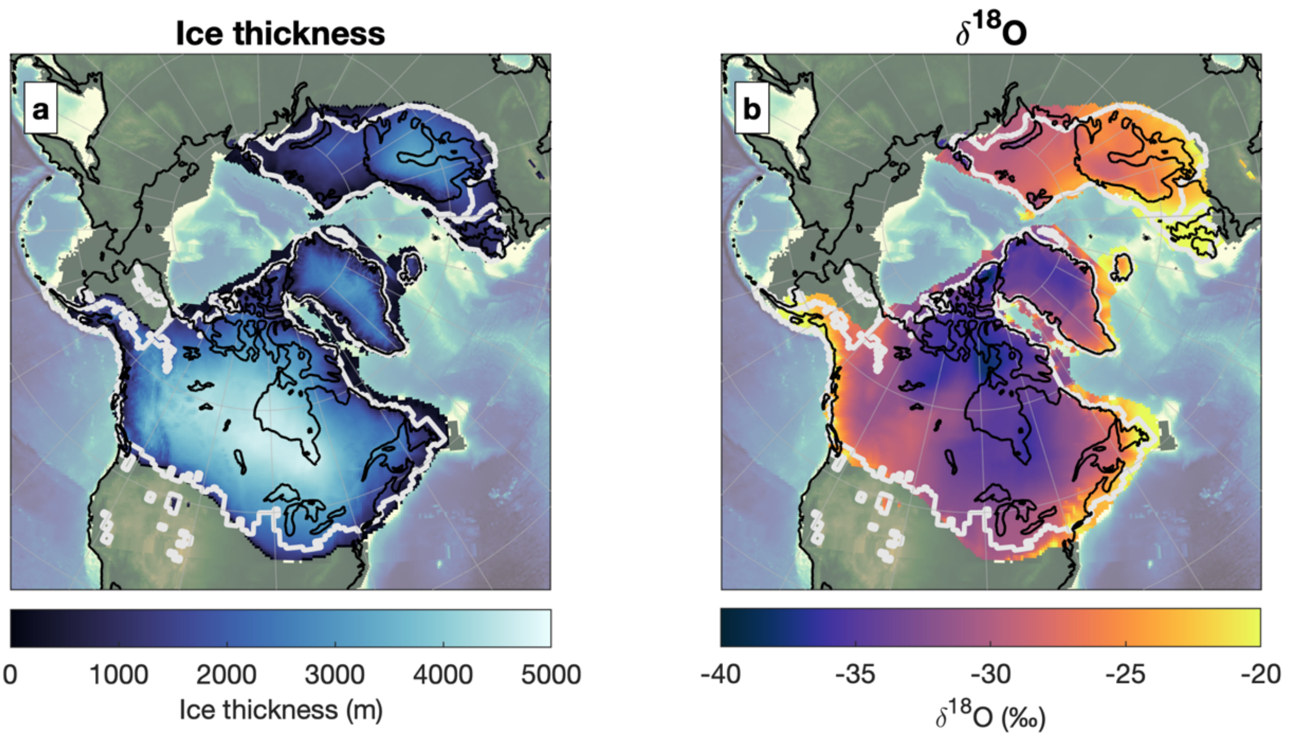

Figure 3. The modelled ice thickness (a), and englacial δ^{18}O (b) at 20 kyr ago in the baseline simulation. The reconstruction of the extent by Peltier et al. (2015) is shown as white contours. The present-day coastline is shown in black.

Fig. 3 shows that the LGM ~~extent is captured by the model. The δ^{18}O~~ice extent reasonably matches the ICE6G ice volume reconstruction by Peltier et al. (2015; see white contours). The englacial δ^{18}O (Fig. 3b) is less depleted where temperatures are high and elevation is low, such as the margins. Fig. 4 shows time-series of the prescribed summer insolation (a), CO_2 (b), the modelled sea level change (c), and benthic δ^{18}O (d), which are compared to reconstructions by Spratt and Lisiecki et al. (2016), Rohling et al. (2021) and Ahn et al. (2017). ~~We always add 20% to~~ In this figure, the modelled sea-level change ~~to approximate~~is increased by 20% to reflect processes that were not explicitly modelled, such as ice volume changes in Antarctica, and temperature/density changes of the ocean. ~~This first-order approximation, which~~This is justified by the strong correlation between global climate, Northern Hemisphere ice volume, and Antarctic ice volume (Gomez et al., 2020), ~~but~~and does not account for out-of-phase behaviour between the Northern and Southern Hemisphere. Additionally, low benthic δ^{18}O and high sea-levels cannot be simulated as we do not include Antarctica.

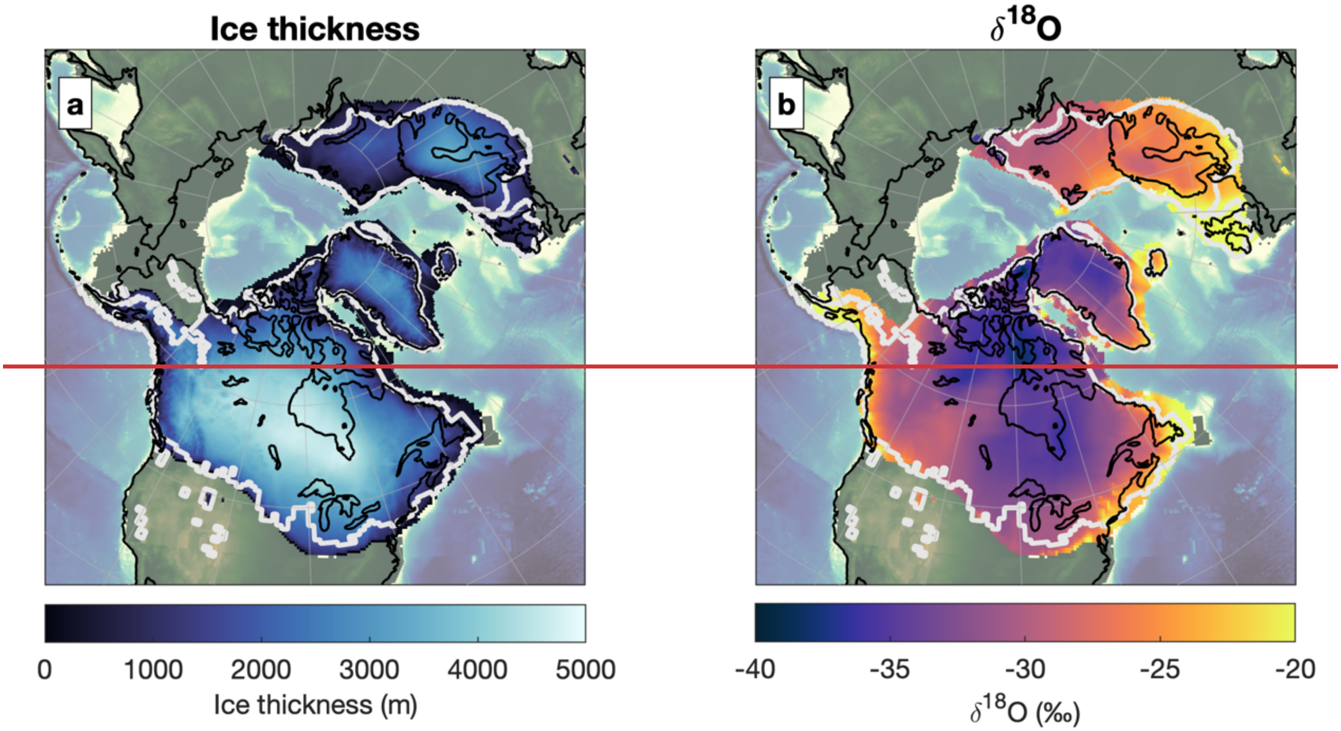

Ice thickness
δ^{18}O
a
b
0
1000
2000
3000
4000
5000
Ice thickness (m)
-40
-35
-30
-25
-20
δ^{18}O (‰)

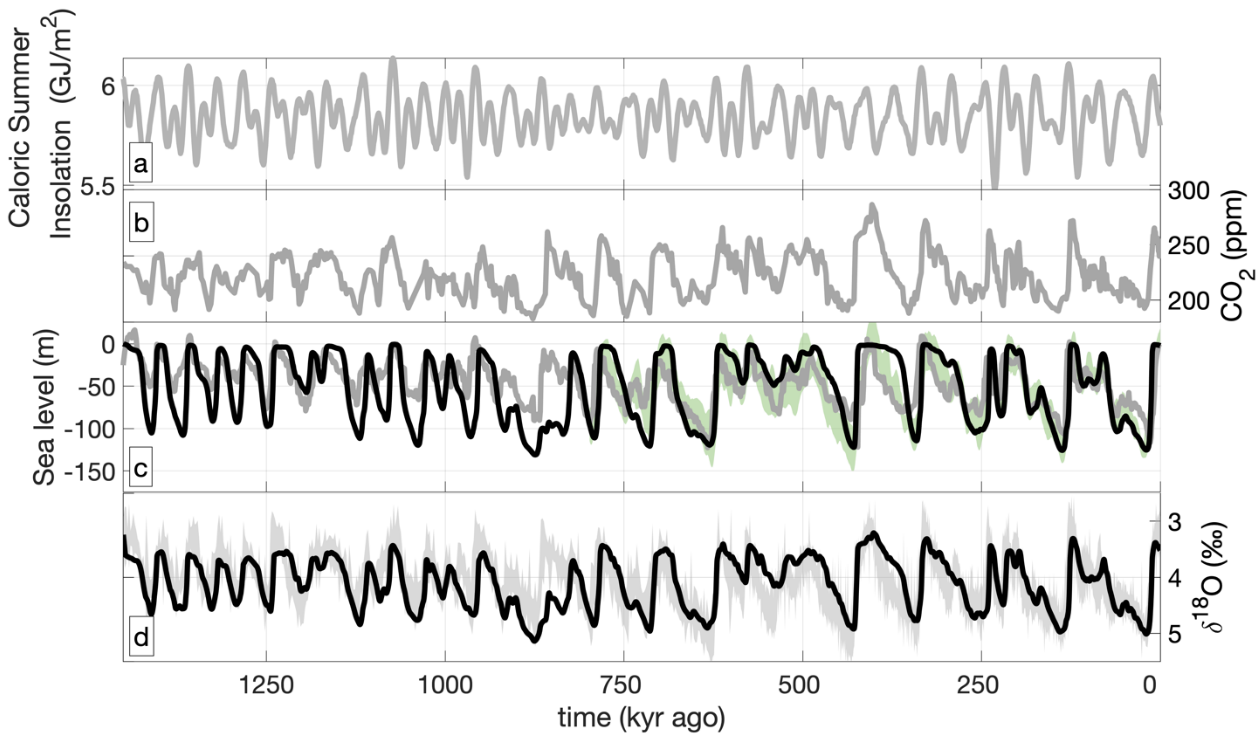

Caloric Summer Insolation (GJ/m^2)
6
5.5
a
b
300
250
200
CO$_2$ (ppm)
Sea level (m)
0
-50
-100
-150
c
d
3
4
5
δ^{18}O (‰)
1250
1000
750
500
250
0
time (kyr ago)

Figure ~~4~~3. ~~The~~. Time-series of the past 1.5 million years ago showing prescribed caloric summer half-year insolation (a) prescribed CO_2 forcing (b), sea level (c) and benthic $\delta^{18}O$ (d). Black lines show modelled sea level (c) and benthic $\delta^{18}O$ (d) of the baseline simulation. Gray shows the reconstructions of caloric summer half-year insolation by Tzedakis et al., (2017; a), CO_2 by Yamamoto et al., (2022; b) sea level by Rohling et al. (2021; c), and $\delta^{18}O$ by Ahn et al. (2017; d). In green (c), sea level reconstruction by Spratt and Lisiecki et al. (2016). Note that lines in grey and green represent reconstructions, while black represents model output.

~~ice thickness (a), and englacial $\delta^{18}O$ (b) at 20 kyr ago in the baseline simulation. The reconstruction of the extent by Pelter et al. (2015) is shown as white contours. The present-day coastline is shown in black.~~

~~We find that the baseline and baseline_icecore simulations capture most of the glacial-interglacial variability over their time-periods. During their overlapping period, baseline and baseline_icecore match reasonably well. The average absolute difference in ice volume is 13 m.s.l.e. (meters sea level equivalent), reflecting the in-phase characteristics of the two CO_2 records (see Yamamoto et al., 2022).~~

~~Peak Northern Hemisphere ice volume during 1500-1000 kyr ago is only a little bit smaller (79±15 m.s.l.e.) compared to the 500-0 kyr ago (98±7 ms.l.e.). Though, at the same time, Early Pleistocene $\delta^{18}O$ levels at glacial maxima are often higher compared to the reconstruction by Ahn et al. (2017). Low benthic $\delta^{18}O$ and high sea-levels cannot be simulated as we do not include Antarctica.~~

The baseline simulation captures the $\delta^{18}O$ variability of most glacial cycles except for the termination at ~865 kyr (MIS 21), where we simulate partial retreat of the North American ice sheet instead of a full deglaciation. CO_2 is low during the 866 kyr ago insolation peak, but rises while insolation strength decreases. Therefore, insolation compensates the rise in CO_2, preventing a deglaciation. ~~Nevertheless, as our baseline simulations captures the main glacial-interglacial variability during the past 1.5 million years, we can explore the cause behind the MPT in more detail.~~

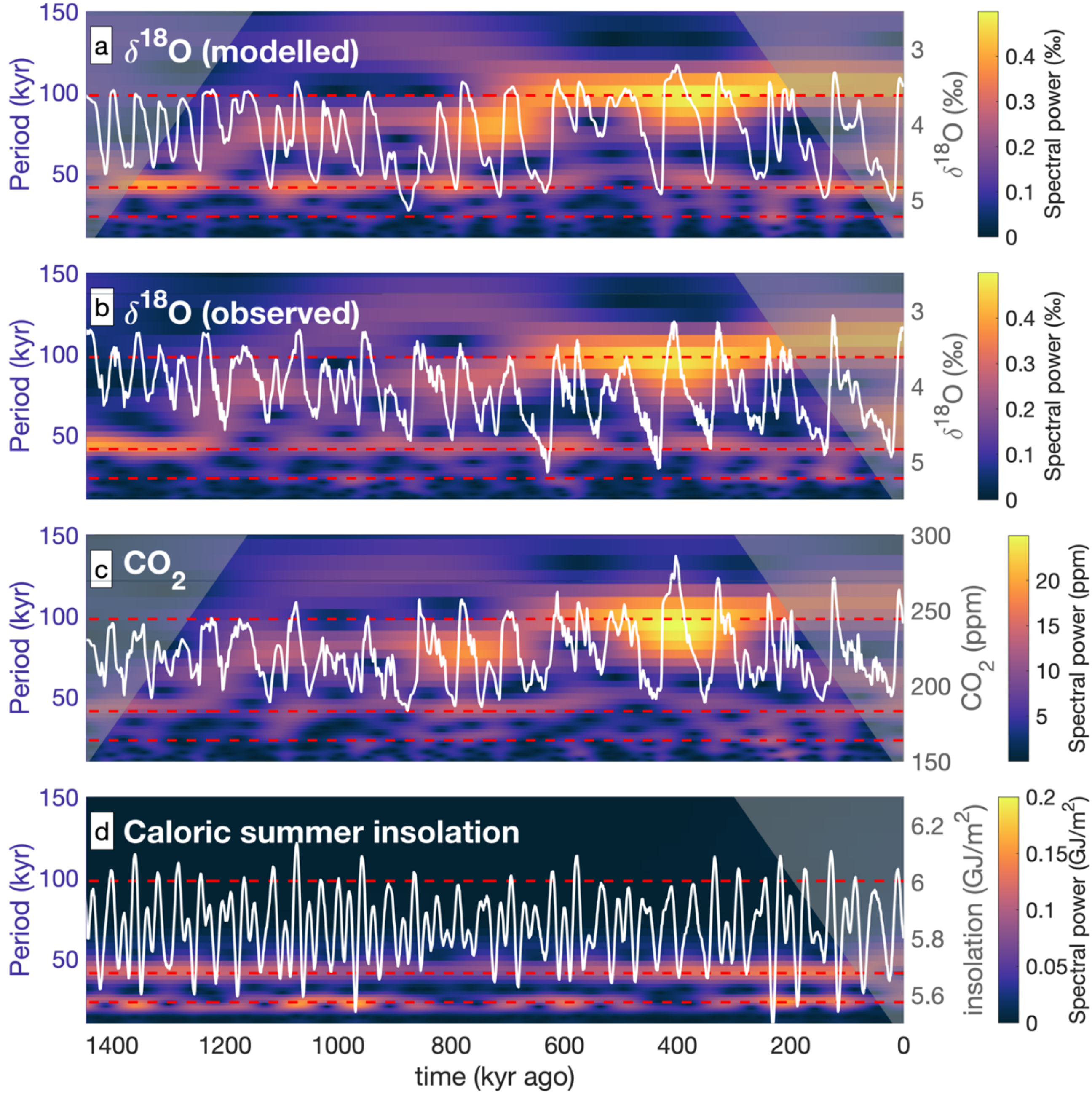

Figure 5. Wavelets transforms showing the explained variance and frequency of the modelled δ^{18}O (a), observed δ^{18}O (Ahn et al., 2017; b), CO_2 (Yamamoto et al., 2022; c) and caloric summer half-year insolation (Tzedakis et al., 2017; d) of the past 1.5 million years. Corresponding time-series are shown in white (see right y-axis). Red dotted horizontal lines indicate 98 kyr, 41 kyr and 23 kyr periodicities, representing eccentricity, obliquity and precession.

Our baseline simulation captures the Late Pleistocene ice volume amplitude, but does not simulate a substantial change in amplitude during the past 1.5 million years. Average glacial peak Northern Hemisphere ice volume during 1,500-1,000 kyr ago is only slightly smaller (79±15 m.s.l.e; m sea level equivalent) compared to the 500-0 kyr ago (98±7 m.s.l.e.).

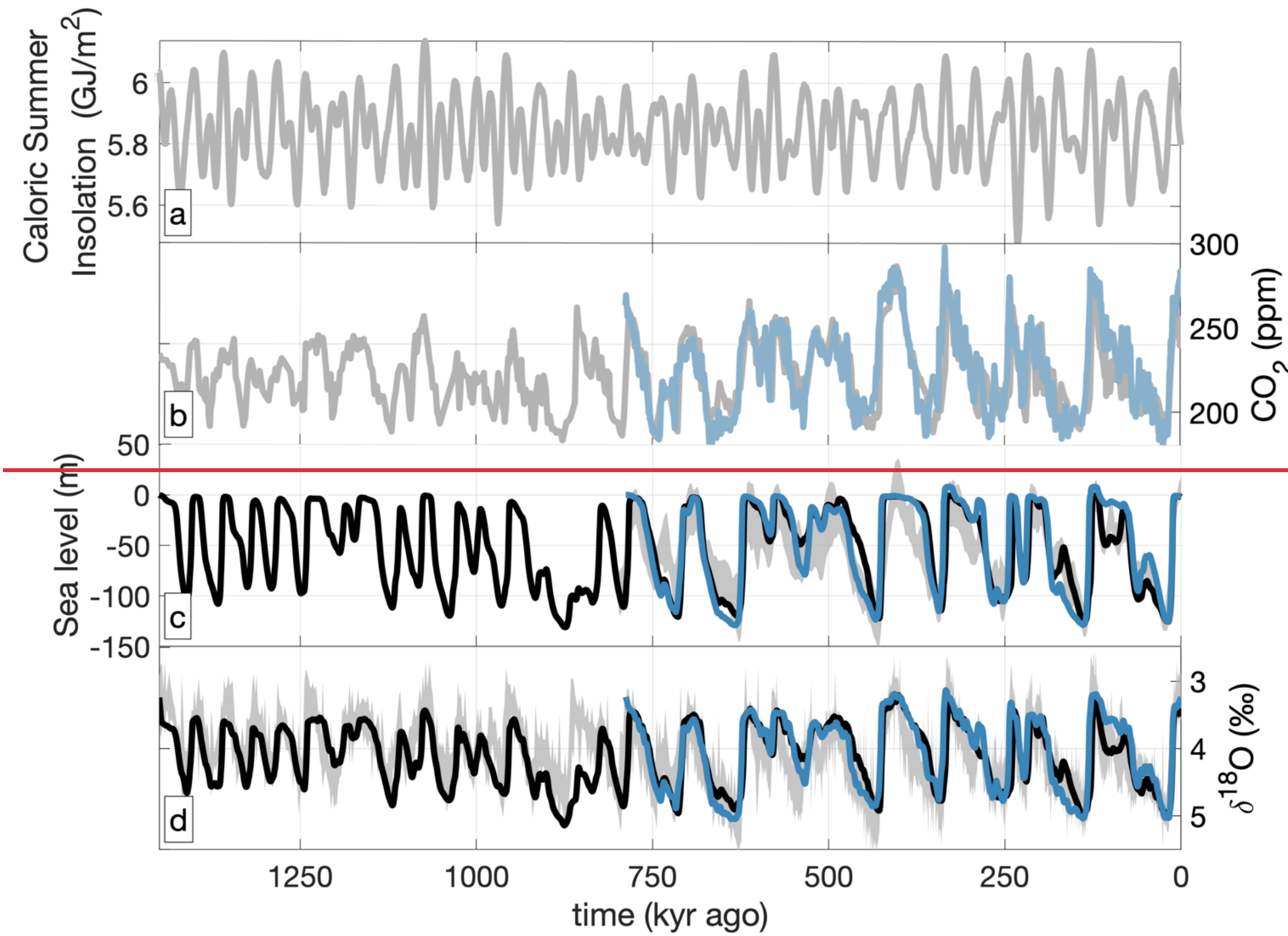

~~**Figure 4.** Time series of caloric summer half year insolation (a), prescribed CO_2 forcing (b) from ice core (blue; Bereiter et al., 2015) and leaf wax (grey; Yamamoto et al., 2022). Sea level (c) and benthic $\delta^{18}O$ (d) of the baseline (black) and baseline_ice core (blue) simulations. In grey, the reconstructions of caloric summer half year insolation by Tzedakis et al., (2017; a), sea level by Spratt and Lisiecki, (2016; c), and $\delta^{18}O$ by Ahn et al. (2017; d).~~

At the same time, Early Pleistocene $\delta^{18}O$ and sea levels at glacial maxima are often higher compared to the reconstructions by Ahn et al. (2017) and Rohling et al. (2021). To test if this large Early Pleistocene amplitude results from the relatively high present-day basal friction, we conduct a sediment_change simulation (see Fig. S2), where we apply homogeneous low “sediment” friction to the Early Pleistocene (until 800 kyr ago). This simulation has a similar glacial-interglacial periodicity as the baseline, but shows a ~10% reduction in amplitude in the Early Pleistocene relative to the baseline. The reduced friction also makes the ice sheet more prone to collapse resulting in full deglaciation at 865 kyr ago, while the baseline does not.

255 As our baseline simulations captures the main glacial-interglacial periodicity during the past 1.5 million years, we can explore the mechanisms behind the MPT in more detail.

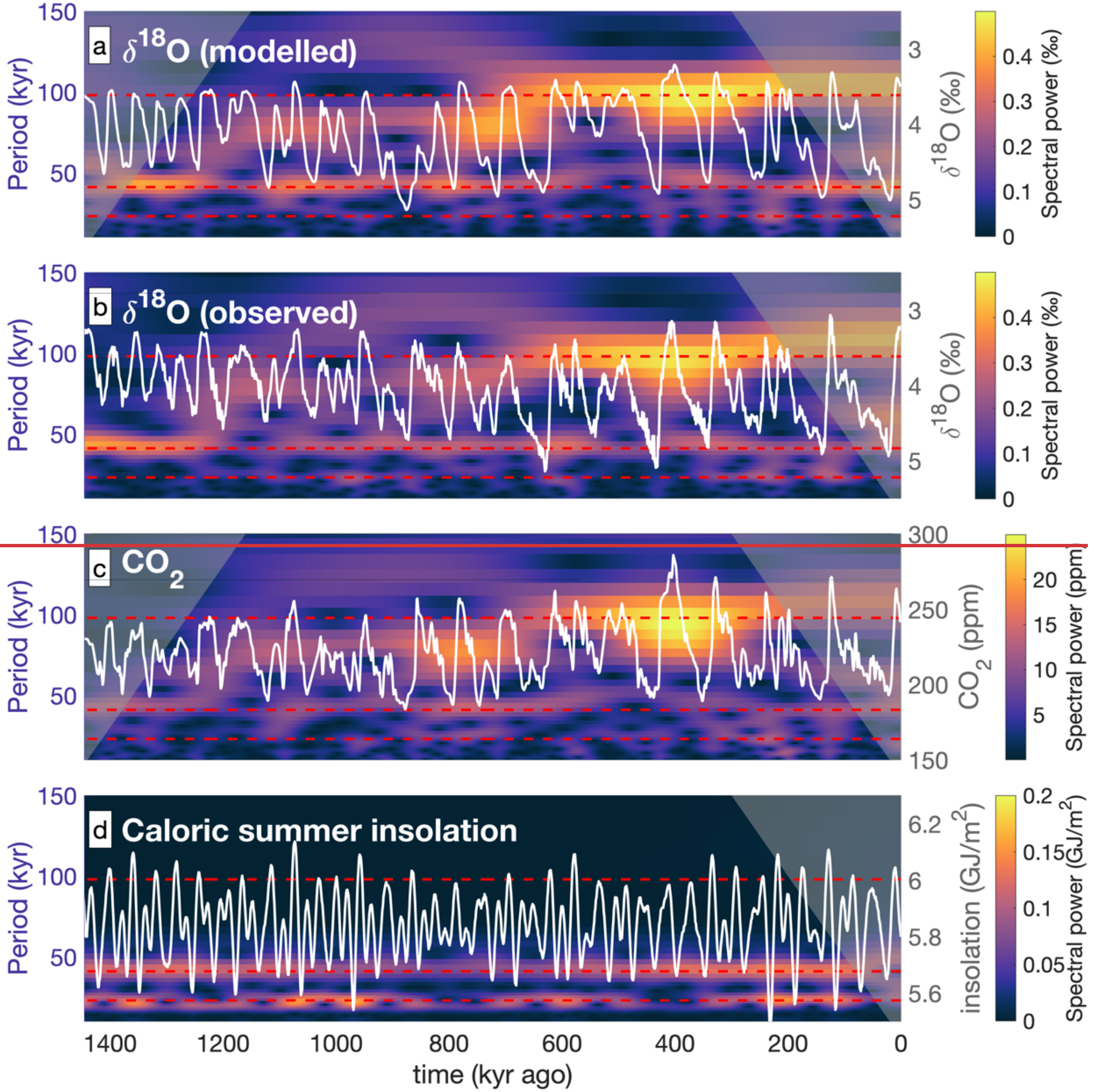

~~Figure 5. Wavelets showing the explained variance and frequency of the modelled δ18O (a), observed δ18O (Ahn et al., 2017; b), CO_2 (Yamamoto et al., 2022; c) and caloric summer half-year insolation (Tzedakis et al., 2017; d). Corresponding time-series are shown in white. Red dotted horizontal lines indicate 98 kyr, 41 kyr and 23 kyr periodicities.~~

3.2 Mechanisms behind the Mid-Pleistocene Transition

In the previous paragraph we showed that we can capture the glacial-interglacial ~~variability~~periodicity in the baseline simulation~~, without any change in basal friction~~. In this section we explore the key elements of the frequency change in our baseline simulation.

Fig. 5a shows a wavelet transform of our modelled $\delta^{18}O$ and compares it to the observed record (Fig. 5b). Our simulation generates the transition from 41-kyr to 100-kyr glacial cycles~~.~~, though with only a small change in glacial-interglacial ice volume difference. The periodicity in the baseline simulation results from the prescribed insolation and CO_2 forcing, combined with ice sheet feedbacks. ~~There is no change in model-setup or any change in basal friction.~~ Since the orbital cycles alone cannot explain all characteristics of the MPT~~,~~ (see Legrain et al., 2023), the main culprit behind our modelled MPT must be the prescribed CO_2 forcing combined with ice-sheet feedback processes.

We can compare the frequency spectrum in the modelled benthic $\delta^{18}O$ to the prescribed caloric summer insolation and CO_2 that drive the modelled temperature change. Fig 5c and 5d show wavelets of the caloric summer insolation and CO_2 forcing. The caloric summer insolation has a strong ~20 kyr and 41 kyr periodicity, corresponding to precession and obliquity respectively. The CO_2 forcing has a weak signal in the 41 kyr periodicity, but a strong 100 kyr signal in the Late Pleistocene. This change in frequency takes place when the modelled $\delta^{18}O$ also changes from 41 kyr to an average 100 kyr.

These results suggest a regime shift between the Early and Late Pleistocene. The 41 kyr periodicity of the Early Pleistocene is generated by the orbital cycles, as the ice sheet melts during strong summer insolation, which tends to correlate with obliquity maxima. The Late Pleistocene is more dominated by CO_2, though still paced by the orbital cycles. Terminations take place if both CO_2 and insolation are high enough, while low interstadial CO_2 levels can sometimes ~~cancel~~partially compensate the strong summer insolation (e.g., ~~461~~ 737, ~~and~~ 175 and 50 kyr ago~~). This would suggest that the MPT could be explained by a decrease of~~), leading to prolonged glacial ~~CO_2 levels~~periods.

~~However, when a Late Pleistocene termination does take place, CO_2 levels have continued to decrease. CO_2 levels rise during terminations, but this rise may be a consequence of the termination rather than the root cause. We did not explicitly simulate the carbon cycle, and we therefore cannot assess the origins of the CO_2 rise, but we can investigate the feedback processes leading to the melt of the ice sheets.~~

Besides the climate forcing (CO_2 and insolation), the ice sheets themselves may also play a significant role in determining which insolation maxima lead to interstadials or terminations. Fig. 6a shows the ice volume of the North American ice sheet at the onset of all modelled terminations, as a function of the climate forcing (external forcing index) at that time. The termination onsets are defined as the maxima in the modelled ice volume that preceded an uninterrupted decrease to (near-

) zero ice volume. These onsets therefore represent an integrated mass balance of around zero and a near-equilibrium with the climate forcing, before the integrated mass balance becomes negative. This collection of terminations spans an S-shaped curve, indicating a non-linearity between ice sheet volume and climate forcing. If the ice sheet is small (<20 m.s.l.e.) it starts melting at relative warm climates. This changes above the 20 m.s.l.e. threshold and below the 60 m.s.l.e threshold. Within this regime, a small change in the climate forcing will substantially increase the ice volume threshold for glacial terminations. When exceeding the 60 m threshold, the S-curve gradually levels off again, and at ice volumes exceeding 75 m.s.l.e., any additional cooling will barely increase the ice volume at terminations. Moreover, even under LGM-like conditions, these large ice sheets may start to lose mass, which could eventually lead to a deglaciation.

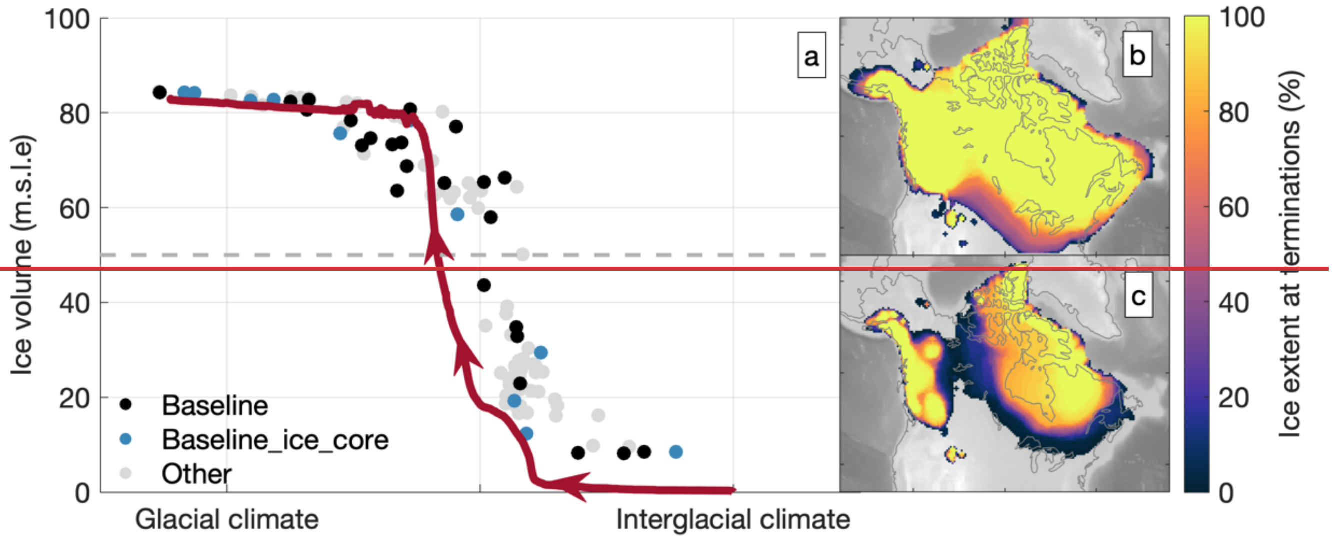

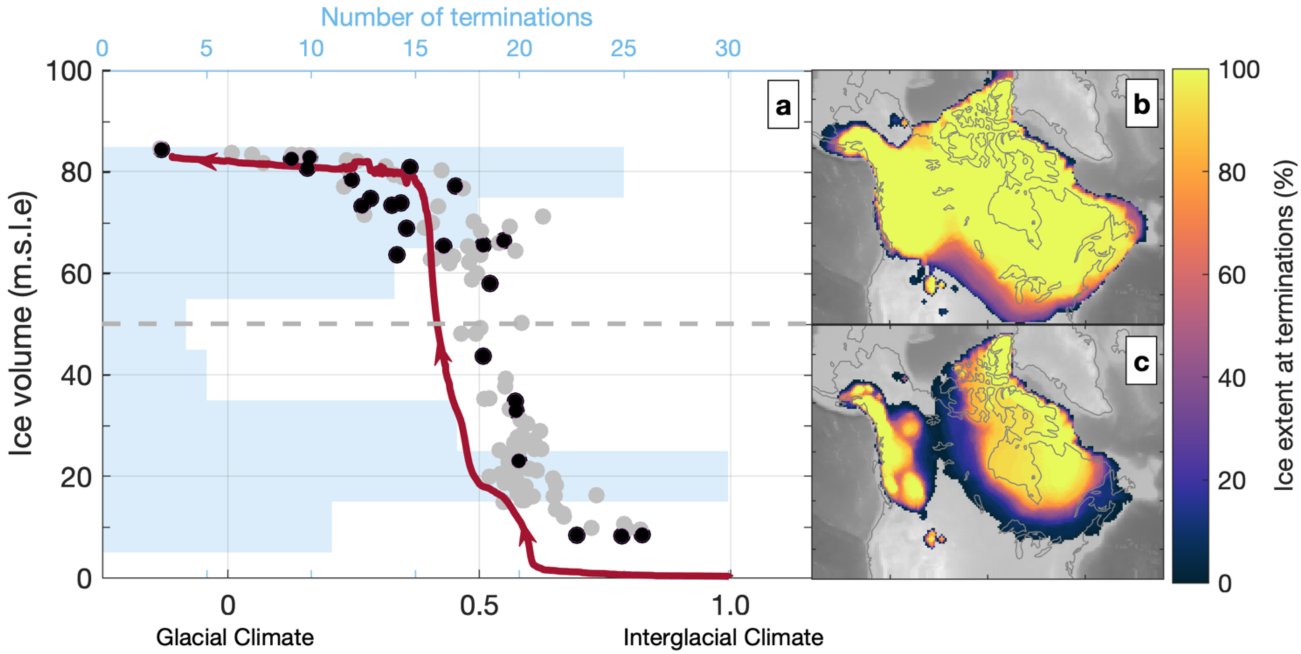

Figure 6. ~~Climate~~Panel a shows the climate forcing (forcing index: insolation and CO_2) and North American ice volume at the onset of deglaciations (a). Black circles represent the baseline simulation, ~~whereas blue is the baseline_ice_core. Grey~~while grey represents the simulations that are introduced in section 3.3 (constant CO_2 or insolation). The red line belongs to the gradual_cooling simulation. In blue, histograms showing the number of terminations per 10 m.s.l.e. ice volume bin. The extent of these terminations is shown in panel (b,c), either with ice volumes above (b) or below 50 m.sl.e. (c~~), with the~~). The colours ~~indicating what~~in b and c indicate which percentage of the ~~landscape was~~terminations in these two groups were covered by ice ~~at~~when the ~~start of the termination~~mass balance became negative. We defined a deglaciation as a continuous melt phase leading to an ice volume of less than 8 m.s.l.e~~.~~ (~10 % of LGM ice volume).

The nonlinearity between ice volume and climate forcing is further ~~confirmed~~explored by the gradual_cooling simulation (see the red line in Fig. 6a), where we gradually altered the climate from interglacial to glacial condition over a period of 1 million years. This simulation provides the ice sheet enough time to readjust to any change in climate forcing, so that it is always (nearly) in equilibrium. As the climate cools, first North-Eastern Canada and the Rocky Mountains will be covered by ice, prompting the first increase in ice volume (<20 m). Afterwards, the majority of growth results from a (high latitude) west-ward expansion of the Laurentide ice sheet, where it has space to grow ~~combined with~~driven by relatively cold climates. The growth of the ice sheet is largely self-sustained by an increase in ice sheet height and albedo, and if allowed to fully adjust to the climate forcing, creates the near vertical profile seen in Fig. 6a. Eventually, the Laurentide and Cordilleran merge together at an ice volume of 54 m.s.l.e, leading to high growth rates due to the merging of ice flows and ablation areas. ~~The strong growth~~This merging may also explain the ~~"gap" between 40 and 55~~relatively low number of terminations around 50 m.s.l.e~~. seen~~., as indicated by the blue histogram in Fig. 6a~~.~~ We can see this in Fig. 6b and 6c, where the extent at the onset of every termination event below or above 50 m.s,l.e. are combined. This 50 m.s.l.e. boundary ~~separates~~groups most of the separated or merged states of the Cordilleran and Laurentide ice sheets. After the merging, the ice sheet cannot migrate west or north, but is forced to thicken or grow to the warmer south, which eventually slows down the growth and prevents further ice expansion.

These results ~~leads to the idea of~~suggest three ~~regimes of~~ ice~~-~~ sheet ~~stability~~volume regimes: a small ice sheet (<25 m.s.l.e.) which easily melts; a medium ice sheet that can grow rapidly through temperature-elevation feedbacks and the merging of the Cordilleran and Laurentide (>25, <~~-~~60 m.s.l.e.); and a large ice sheet (>~~-~~60 m.s.l.e.) which is sensitive to a change in climate due to strong positive melt feedbacks, such as the melt-elevation feedback, melt-albedo feedback and the formation of proglacial lakes (see Scherrenberg et al., 2024) and a thermodynamical decoupling (Bintanja and van de Wal, 2008). A sharp increase in CO_2, combined with the strong summer insolation at glacial terminations could then further accelerate the melt of the ice sheets. ~~A successful~~A successfully modelled termination therefore hinges on whether this melt-feedback loop is triggered. If the ice sheet falls within the large regime, a period with strong summer insolation ~~could~~can more easily trigger the melt feedback loop. CO_2 and insolation conditions for which a small or medium-sized ice sheet could survive, can yield a full collapse of a large ice sheet. Reversely, if the combination of CO_2, insolation and ice volume fails to trigger strong enough melt-feedback processes, the ice sheets do not fully melt, prolonging of the glacial period.

~~This may also explain why the Late Pleistocene glacial terminations only take place during some, but not all, insolation maxima. Low CO_2 levels may cause an insolation maximum to be skipped if the ice-sheet is medium-sized, but even lower CO_2 concentrations can still generate a full collapse if the ice sheet is large-sized. The periodicity of the benthic $\delta^{18}O$ record is then dominated by the successful terminations, which only occur when the combination of insolation, CO_2 and ice volume is right to trigger a strong enough melt-feedback loop.~~

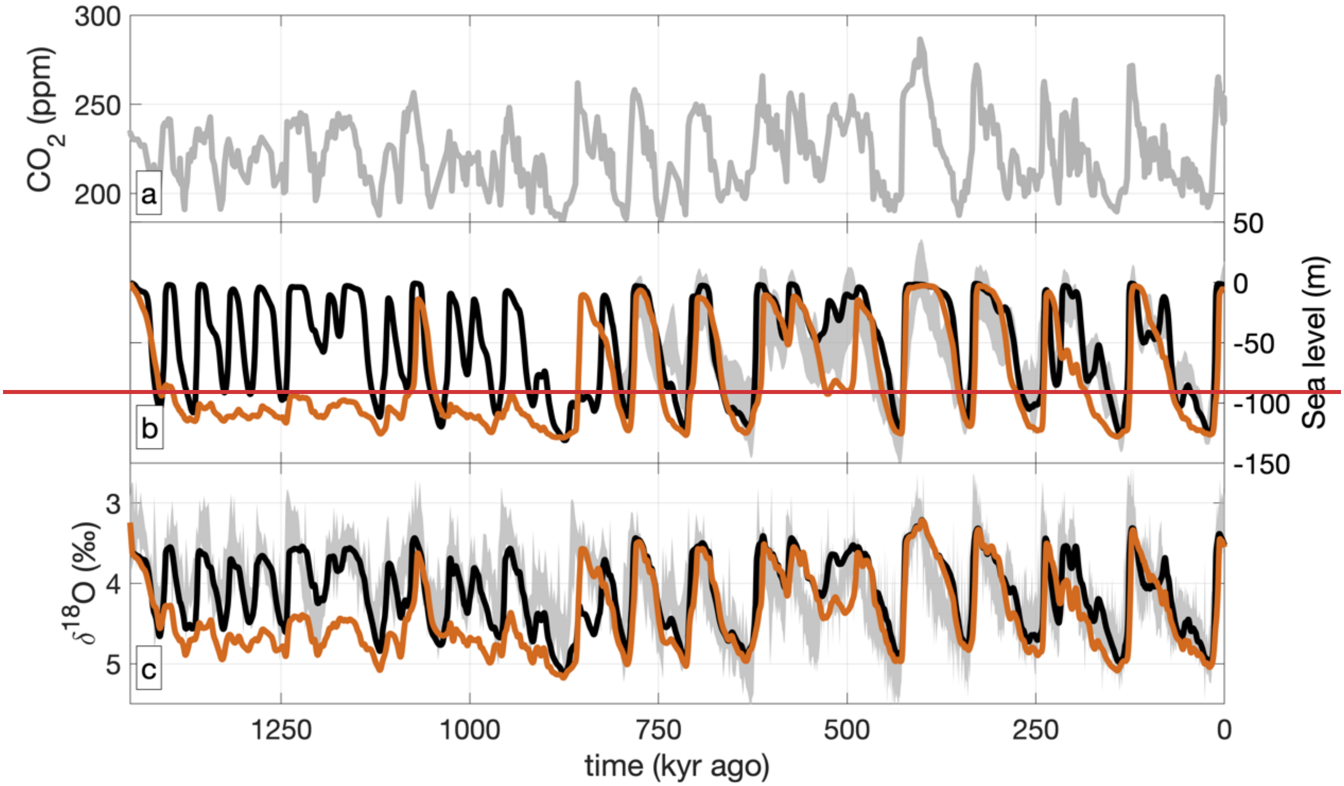

~~**Figure 7.** Time series of prescribed [MOU1][Rv2][Rv3]CO_2 (a), sea level (b), $\delta^{18}O$ (c) and of the baseline (black) and constant_insolation (orange) simulations. Reconstructions by Yamamoto et al. (2022; a), Spratt and Lisiecki (2016; b), and Ahn et al (2017; c) are shown in grey.~~

3.3 Disentangling CO_2 and insolation

Our baseline simulation can capture the frequency change during the MPT using prescribed changes in CO_2 and summer insolation. In this section, we ~~will~~ explore the model response if either one is removed.

~~In the~~ We conduct four constant_insolation simulations by applying the constant insolation at 0 kyr ago, (implying a constant caloric summer insolation of ~5.8 GJ/m^2), 5 kyr ago ("enhanced" insolation; ~5.9 GJ/m^2), 25 kyr ago (insolation minimum; ~5.4 GJ/m^2), and 10 kyr ago (insolation maximum; ~6.1 GJ/m^2). Note that the caloric summer insolation at 0 kyr ago is close to the mean of the past 1.5 million years (5.84 GJ/yr). Each constant_insolation simulation~~,~~ has the same set-up as the baseline, but we apply ~~the present-day~~a constant (monthly varying) insolation ~~(implying a constant caloric summer insolation of 5.8 GJ/m^2) to the baseline set-up. In this simulation, temperature~~. Temperature change results only from CO_2 and the albedo feedback. Note that the resulting glacial periodicity can still match orbital cycles, as past CO_2 levels were not independent from insolation.

Time-series of modelled sea level and benthic $\delta^{18}O$ in the constant_insolation and baseline simulations are shown in Fig. 7. ~~Constant~~Three out of four constant_insolation ~~does~~do not capture the Early Pleistocene glacial cycles, ~~as the relatively~~

while the constant_insolation_5kyr_ago matches the glacial-interglacial periodicity during the Pleistocene, though with long interglacial periods during the Late Pleistocene.

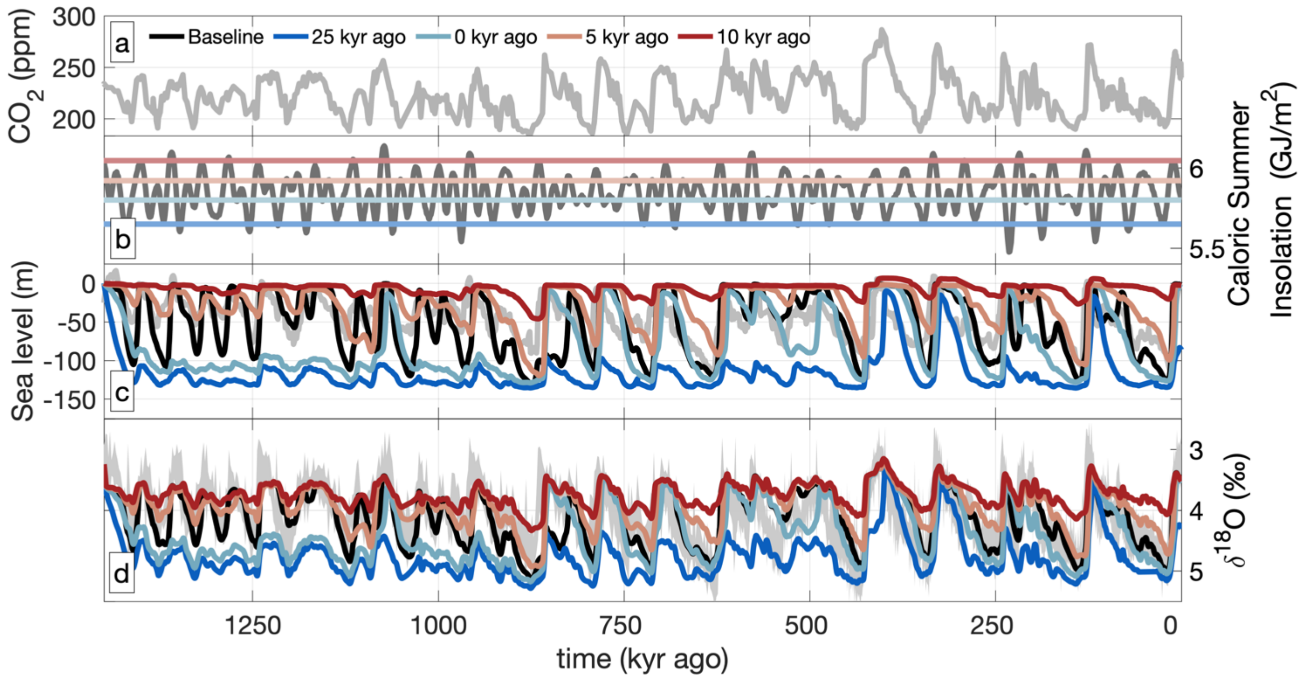

Figure 7. Time-series of prescribed CO_2 (a), insolation (b), sea level (c) and $\delta^{18}O$ (d). CO_2 reconstruction by Yamamoto et al. (2022; a), sea-level by Rohling et al. (2012; c), and $\delta^{18}O$ Ahn et al (2017; d) all shown in grey.

Whether the constant_insolation simulations match the periodicity depends on interglacial CO_2 levels and the constant insolation strength. In the Yamamoto et al. (2022) record, interglacial CO_2 levels are low ~~CO_2 levels~~ during the Early Pleistocene (~240-250 ppm) ~~fail to initiate a termination in combination with the present-day insolation. The Late Pleistocene interglacial periods have higher CO_2 levels (>250 ppm), and as such, the~~ and increase during the Late Pleistocene, with high interglacial CO_2 levels during the past 400 kyr (~260-270 ppm). If summer insolation is weak (constant_insolation_0kyr_ago/25kyr_ago), only some Late Pleistocene cycles are captured. If summer insolation is relatively strong (constant_insolation_5kyr_ago), the low interglacial CO_2 levels during the Early Pleistocene can trigger terminations ~~are modelled and our simulation has a closer match with reconstructions. This may suggest that the system is more driven by changes in CO_2 during this time. It also indicates that, even if a simulation produces a good match with reconstruction for the last few glacial cycles, there is no guarantee it will do so for the entire Pleistocene~~. Very strong summer insolation (constant_insolation_10kyr_ago) prevents the growth of ice and the ice volume stays below the “small” threshold regime.

~~These results indicate that CO_2 alone is not capable of explaining the glacial-interglacial variability of the past 1.5 million years, especially the Early Pleistocene glacial cycles. Therefore, to~~To investigate if orbital cycles alone can capture the MPT in our set-up, we conduct simulations with constant CO_2 instead. As such, there is no change in CO_2 concentration for glacial, interstadial or interglacial periods.

Fig. 8b shows sea level time-series of simulations forced by constant 240, 220 and 210 ppm CO_2 concentrations (constant_CO2 experiments). The modelled ice volume differs substantially between these three simulations: Constant_CO2_240 yields small ice volumes (generally less than 50 m.s.l.e.), which is around half of that in the constant_CO2_220 and constant_CO2_210 simulations. The ice ~~sheet~~sheets in the constant_CO2_240 simulation mostly melts at 41-kyr intervals. The constant_CO2_220 largely follows the glacial-interglacial periodicity during the Early Pleistocene, and also captures some of the termination events and prolonged glacial periods during the Late Pleistocene. Constant_CO2_210 has an even lower CO_2 concentration, leading to long glacial cycles. In all these simulations, the ice sheets can still fully melt, despite ~~these~~ low constant CO_2 concentrations. This is facilitated by ~~strong~~ positive melt feedbacks ~~and~~combined with strong summer insolation.

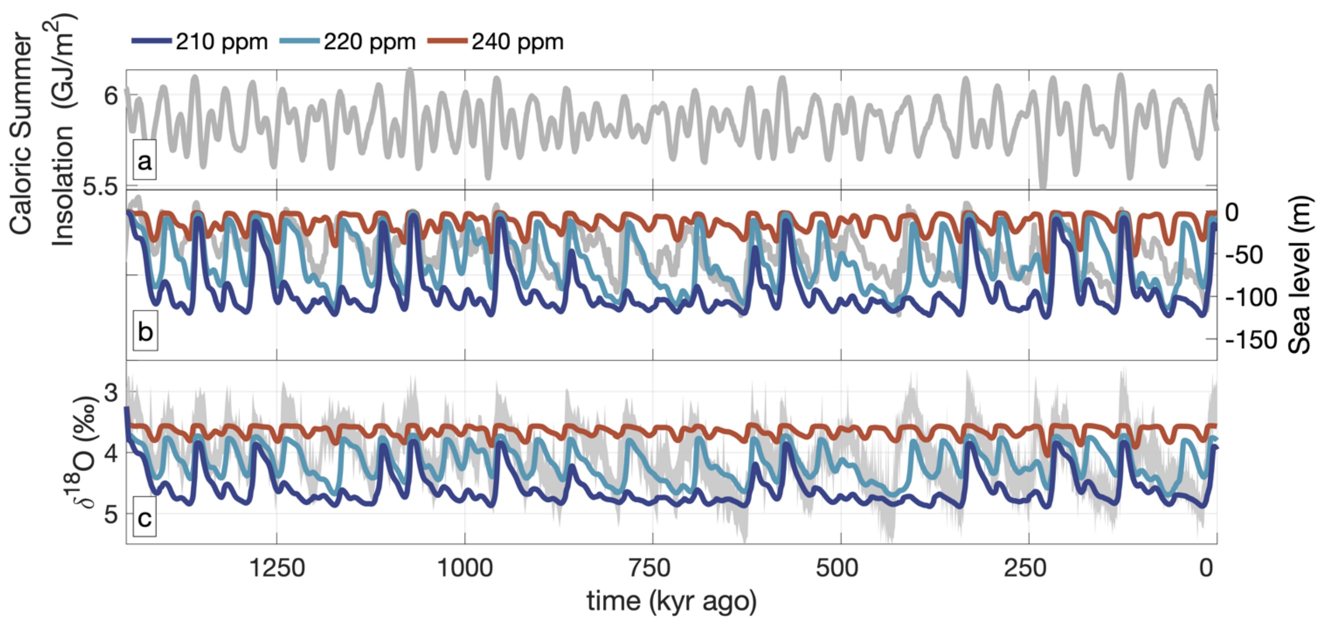

Figure 8: Time-series of caloric summer half-year insolation (a), sea level (b), and $\delta^{18}O$ (c) of the experiments with constant 240 ppm (red), 220 ppm (cyan) and 210 ppm (blue) CO_2 levels. Observed sea level (Spratt and Lisiecki, 2016; b) and $\delta^{18}O$ (Ahn et al., 2017; c) is shown in grey. Note that the $\delta^{18}O$ of sea water is calculated using CO_2, and all variability of $\delta^{18}O$ in the constant_CO2 simulations therefore results from the ice sheets.

Fig. 9 shows wavelet transforms of the sea level and compares it to the summer insolation, which represents the only driver of temperature change in the constant CO_2 simulations. Constant_CO2_240 and constant_CO2_220 simulations show 41-kyr periodicity during the Early Pleistocene, but this generally persists into the Late-Pleistocene. While constant_CO2_220 and constant_CO2_210 ~~can have~~show increased periodicity when insolation maxima are skipped, neither ~~show~~maintain a prolonged 100-kyr periodicity~~. Therefore, the constant_CO2 experiments are almost the reverse of the constant_insolation:~~

~~Constant CO_2 levels can largely capture the periodicity during the Early Pleistocene glacial cycles, while constant insolation captures the Late Pleistocene instead. These results also suggest that a gradual decrease of glacial CO_2 could prolong glacial periods. With decreasing CO_2 concentrations, fewer insolation maxima lead to terminations, which increases the duration of glacial cycles. A gradual decrease in glacial CO_2 levels could therefore explain the MPT~~.

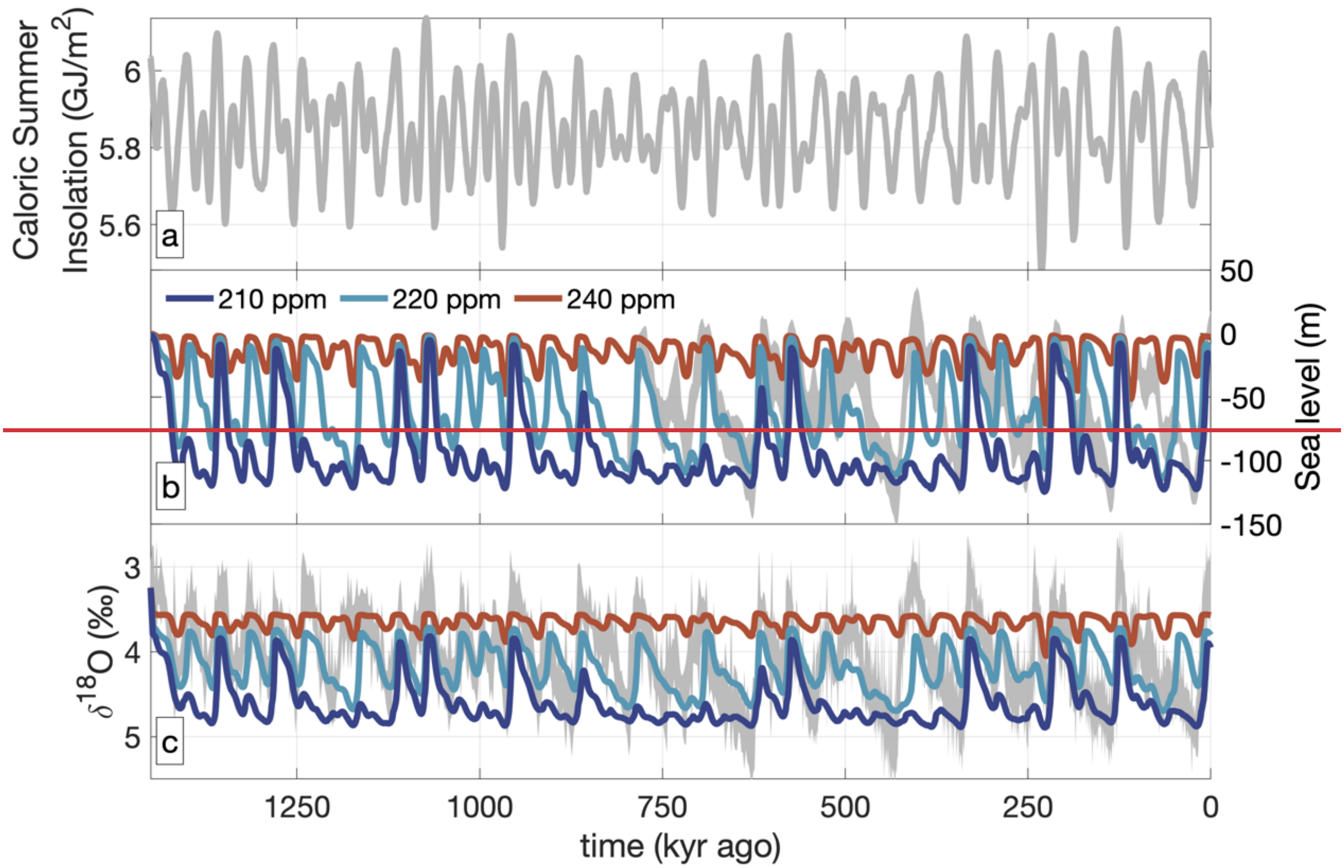

~~**Figure 8:** Time-series of caloric summer half-year insolation (a), sea level (b), and $\delta^{18}O$ (c) of the experiments with constant 240 ppm (red), 220 ppm (cyan) and 210 ppm (blue) CO_2 levels. Observed sea level (Spratt and Lisiecki, 2016; b) and $\delta^{18}O$ (Ahn et al., 2017; c) is shown in grey. Note that the $\delta^{18}O$ of sea water is calculated using CO_2, and all variability of $\delta^{18}O$ in the constant_CO2 simulations therefore results from the ice sheets.~~

~~Remarkably, while~~While precession is present in the climate forcing (Fig. 9d), the ~20-kyr signal is mostly absent in the frequency spectrum of the modelled sea level. Terminations are initiated when insolation is strong enough to initiate positive melt feedbacks. The insolation threshold for a termination depends also on CO_2, as the constant_CO2_240, 220 and 210 simulations ~~tend to~~generally melt at a caloric summer half-year insolation of roughly 5.9 GJ/m^2, 6.0 GJ/m^2 and 6.1 GJ/m^2 respectively. The terminations tend to occur during peaks in the caloric insolation (generally obliquity), while many smaller peaks (mostly precession) are skipped. Additionally, we have used caloric summer insolation as a driver for temperature change, which accounts for a change in the duration of the melt season that is caused by, and partly compensates the precession signal (see Huybers, 2006). Terminations will therefore tend to correlate to obliquity maxima and filter out precession. ~~This idea, that a threshold in caloric summer insolation can generate precession cancellation, has also been suggested by Tzedakis et al. (2017). Here we find that the feedback processes in the Northern Hemisphere ice sheets (e.g., albedo and topography) can filter out the precession signal. This would also suggest that the glacial cycles of the Early Pleistocene were always paced by all orbital cycles. However, only the stronger peaks (generally obliquity) in summer insolation can prompt the melt feedback loop, filtering out the weaker insolation maxima (generally precession).~~ The resulting ice volume frequency spectrum will then be dominated by the successful terminations.

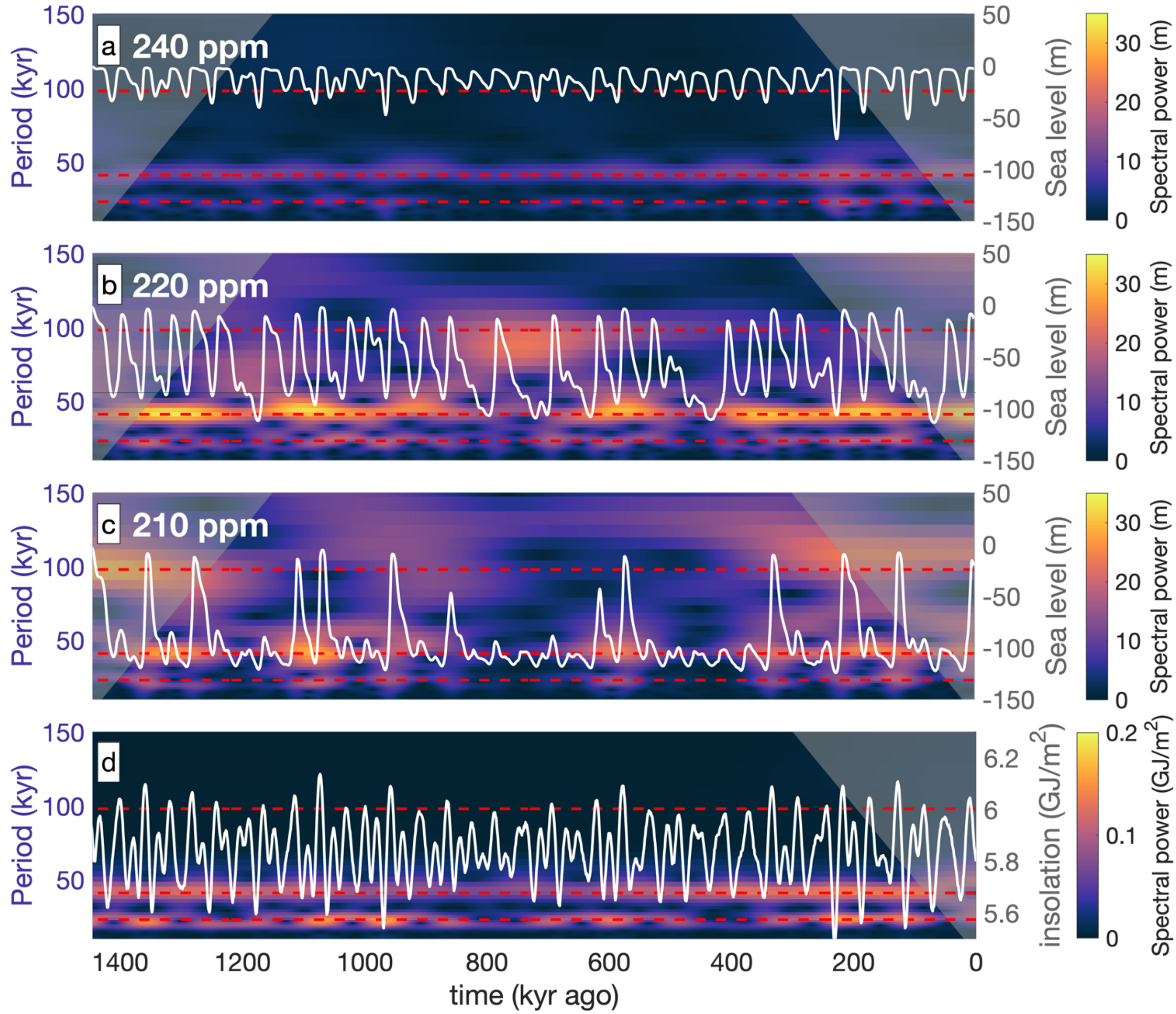

Figure 9. Wavelets showing the frequency in the sea level of 240 ppm (a), 220 ppm (b) and 210 ppm (c), compared to caloric summer half-year insolation (d). Corresponding time-series are shown in white.

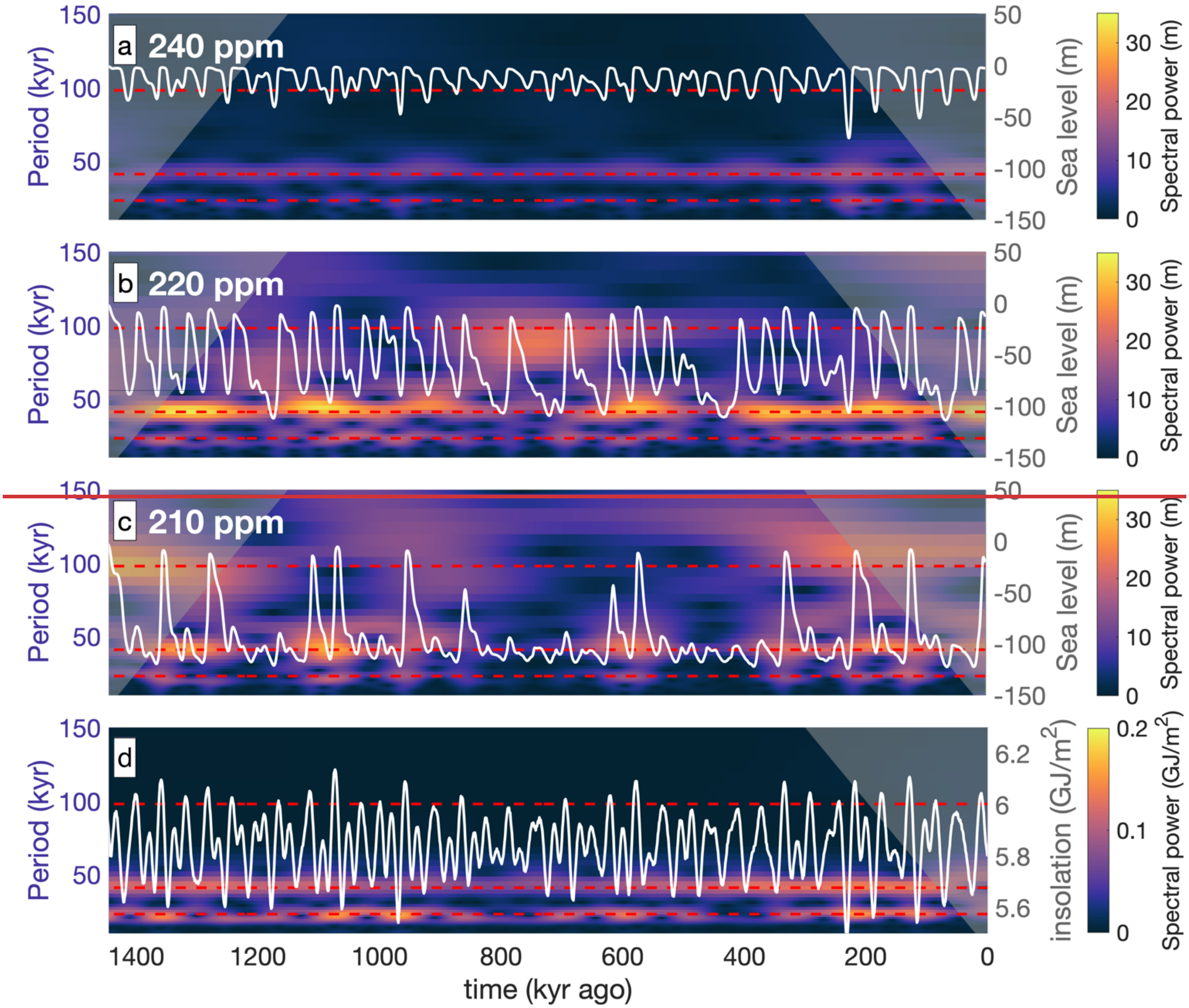

~~**Figure 9.** Wavelets showing the frequency in the sea level of 240 ppm (a), 220 ppm (b) and 210 ppm (c), compared to caloric summer half-year insolation (d). Corresponding time series are shown in white.~~

4. Discussion

In this study we simulate the 1.5-million-year Northern Hemisphere ice-sheet evolution ~~during the past 1.5 million years~~ using ~~a~~ climate forcing ~~that depend on~~driven by prescribed CO_2~~,~~ and insolation~~,~~ and implicit ice-sheet-climate interactions. Using these driving forces, we are able to capture the glacial-cycle frequency change at the MPT without any change in model-set-up or basal friction. ~~We find that the~~ Our modelled MPT results mainly from ~~a change in amplitude and frequency of~~ the prescribed CO_2 record~~. During the Early Pleistocene, CO_2 is high enough to lead to a termination at every obliquity maximum. However, during~~: In the Late Pleistocene, ~~CO_2 is too~~ low ~~during~~interstadial CO_2 levels are maintained throughout some insolation maxima, ~~resulting in a prolongation of~~prolonging the glacial period~~ and thereby increased periodicity. This idea is further confirmed by simulations with constant CO_2 levels, as more insolation maxima are skipped with decreasing CO_2 concentrations~~.

~~However, at~~ While we do simulate the ~~end of the~~ frequency change and Late Pleistocene ~~terminations, CO_2 levels have continued to decrease, but the ice sheets will still melt. We instead propose that the North American ice sheet itself could play a major role in these terminations. In general, as the climate becomes colder, ice sheets can become larger before it starts to attain a negative mass balance. However, we find certain threshold regimes in the North American ice sheet: A small ice sheet will melt at relatively strong CO_2 and insolation. A medium-sized ice sheet grows towards central Canada until eventually, the Laurentide and Cordilleran ice sheets merge. This facilitates a self-sustained growth of the ice sheets, and a small change in the climate forcing will substantially increase the~~ ice volume~~ threshold for glacial terminations. After this merging~~, we only obtain a ~~large-sized ice sheet that has a long margin in the south. This ice sheet is much more sensitive towards insolation increase, and needs low CO_2 and summer insolation to survive. A low glacial CO_2~~small shift in the sea level ~~can therefore delay a deglaciation of a medium-sized ice sheet, but once the ice sheet is large enough, another insolation maxima may trigger a full termination instead. This is~~amplitude across the MPT. Our simulations are forced by and dependent on the leaf-wax proxy CO_2 record by Yamamoto et al. (2022), which is currently the only continuous CO_2 record of the past 1.5 million years. This record has relatively low Early Pleistocene (inter)glacial CO_2 levels compared to boron-isotope-based records (e.g., see Chalk et al. 2017) and carbon cycle modelling results (e.g., Willeit et al., 2019). If Early Pleistocene CO_2 concentrations are indeed underestimated in the Yamamoto et al. (2022) record, this would lead to temperatures that are too low, and thereby generate a too large ice volume amplitude. Additionally, we applied a constant (present-day) sediment map, leading to too-high friction and consequentially too-large ice volume during the Early Pleistocene.

Our North American ice volume shows a threshold regime: Small ice sheets melt easily. Medium ice sheets are less sensitive due to their location combined with the merging of the Cordilleran and Laurentide ice sheet inducing a positive feedback, in agreement with Bintanja and van de Wal (2008). Large ice sheets have a long southern margin and are sensitive to small increases in temperature. A successful termination hinges on whether the climate forcing (CO_2 and insolation) and ice volume can trigger a strong melt feedback, which is facilitated by melt-elevation feedback and proglacial lakes. These threshold regimes are in line with several studies that suggest that the Late Pleistocene terminations only take place if ice volume is large enough (~~Abe-Ouchi et al., 2013;~~ Parrenin and Paillard, 2003; Bintanja and van de Wal 2008~~,~~; Abe-Ouchi et al., 2013; Verbitsky et al., 2018; Berends et al., 2021a). ~~The resulting frequency spectrum of ice volume will then be~~ Additionally, several studies (see Parranin and Paillard, 2003; Berends et al., 2021a; Legrain et al., 2023) used conceptual models to show that such a threshold behaviour could lead to a change in glacial-interglacial periodicity, here we show the same for a more realistic bed topography and climate.

This threshold behaviour may also explain why the Late Pleistocene glacial terminations only take place during some, but not all, insolation maxima. Low interstadial CO_2 levels may cause an insolation maximum to be skipped if the ice-sheet is medium-sized, but even lower glacial CO_2 concentrations could potentially still generate a full collapse if the ice sheet is large-sized. The periodicity of the benthic δ^{18}O record is then dominated by the successful terminations, which ~~depend whether~~ only occur when the combination of insolation, CO_2 and ice volume are able to trigger a strong enough melt-feedback loop ~~is triggered. These positive melt feedbacks result from the melt-elevation, melt-albedo feedbacks, and the creation of proglacial lakes. Melt rates~~.

These ideas are further ~~enhanced by the increase in CO_2 concentrations. Whether these feedbacks are triggered therefore depends on the climate forcing (CO_2 and insolation) as well as the ice volume of the North American ice sheet.~~

~~To investigate the relative importance of orbital forcing and CO_2, we conducted simulations with either~~explored by simulations that use constant ~~orbital configurations~~CO_2 levels or insolation. Using constant ~~CO_2. If~~ insolation ~~is constant, temperature responds mostly to CO_2, and~~, we ~~can capture the Late Pleistocene terminations, but the Early Pleistocene cycles merge together. If CO_2 levels are constant instead, we can mostly capture the 41-kyr periodicity during the Early Pleistocene, but fail to fully capture the 100-kyr periodicity of the~~ are able to generate the terminations of the Early and Late Pleistocene ~~cycles.~~, though whether these glacial cycles are captured is conditional to a narrow range of constant caloric summer insolation combined with the prescribed interglacial CO_2 levels. If interglacial CO_2 is high (Late Pleistocene), terminations are possible at lower constant summer insolation. If ~~the~~interglacial CO_2 is low (Early Pleistocene, according to Yamamoto et al., 2022), stronger constant ~~CO_2 level is low enough, the length~~ summer insolation is needed for terminations.

If we used constant CO_2 instead, we could capture the 41 kyr cycles of the Early Pleistocene. Using low constant CO_2 levels (220 ppm), we could capture the Early Pleistocene cycles and some Late Pleistocene glacial cycles. However, no persistent 100 kyr periodicity was established. This is partially in line with conceptual model results by Legrain et al., (2023), finding that orbital cycles alone can capture some (but not all) characteristics of the MPT. However, if the carbon cycle was modelled and CO_2 was allowed to freely evolve, the modelled glacial-interglacial frequency could be different. For example, an intermediate complexity model simulation with active carbon cycle component by Willeit et al. (2019) generated a persistent 100-kyr periodicity with only orbital forcing.

The climate forcing of the ~~glacial cycles may increase. We~~constant_CO2 simulations is driven by insolation, which encloses a precession signal. This signal is filtered from the modelled ice volume as deglaciations are only triggered if summer insolation is strong, which tends to filter out the relatively weaker insolation maxima (induced by precession). The resulting ice volume frequency is therefore dominated by obliquity, as only these trigger successful terminations in the Early Pleistocene. This idea, which proposes that a threshold in caloric summer insolation can generate precession cancellation, has also been suggested by Tzedakis et al. (2017). In this study, we have found that the non-linear response of the Northern Hemisphere ice sheet towards climate forcing can filter out the precession signal.

We also found a very strong sensitivity to the constant CO_2 levels, as a decrease from 240 to 220 ppm CO_2 yields a doubling in ice volume. While it is uncertain if this sensitivity fully holds-up in a fully-coupled Earth-System Model set-up, it does partially agree with similar experiments using an intermediate complexity model (see Ganopolski and Calov, 2011). However, their 240 ppm CO_2 level already shows some skipped terminations at obliquity maxima, while ~~this concentration~~our simulation ~~yielded~~ yields a persistent 41-kyr periodicity in our simulation instead.

This high sensitivity to CO_2 also highlights the importance of accurate CO_2 reconstructions to detect the changes in long-term CO_2 concentration over the MPT. We have used a leaf-wax ~~CO_2~~ record (Yamamoto et al., 2022~~),~~) that has (indirectly) reconstructed CO_2, which was calibrated to (directly measured) CO_2 record obtained from air trapped inside ice (Bereiter et al., 2015). ~~has higher~~However, the leaf-wax record has larger uncertainties compared to ice~~-core records (~~ cores,~~Bereiter et al., 2015). These CO_2 records match well during their overlapping period~~ and ~~both are capable of reproducing the glacial-interglacial variability. Although, the~~ as such, CO_2 ~~levels~~records before the ice core (800~~-~~ kyr ago) is still uncertain ~~as continuous ice-core records do not cover this period yet.~~. Nevertheless, the shift from 41 to 100 kyr periodicity in the CO_2 record is also found in boron-based CO_2 reconstructions (e.g., Dyez et al., 2018~~), indicating that this~~). Therefore, the frequency shift in CO_2 is consistent among different CO_2 records. ~~Additionally, both Yamamoto et al. (2022) and Hönisch et al. (2009) find a decrease in glacial CO_2 concentrations across the MPT. Our~~Our Early Pleistocene from our baseline simulation results ~~also~~generally agree with Watanabe et al. (2023), who found based on ice-sheet model simulations that the Early Pleistocene glacial cycles follow from orbital oscillations, with minimal effect from CO_2. We were however able to capture the Early Pleistocene cycles using either constant CO_2 levels or a narrow range of constant insolation.

~~In order to simulate~~Simulating 1.5 million years requires a trade-off between explicitly modelling processes and computational time. While we simulate some ice-sheet climate interactions, they are more complex in reality. For example, we do not include any feedback from the ocean circulation or sea ice. Another limitation of our approach is that the climate forcing is only based on just two ensemble-mean climate time-slices. This choice was made due to the large differences between climate models, whereas the PMIP4 ensemble shows good results (see Kageyama et al., 2021). These GCM simulations were conducted with a prescribed LGM ice sheet, and the high albedo of the ice sheet leaves a cold imprint on the temperature field and creates a large temperature gradient between ice and ice-free areas. If the ice volume is close to LGM, the extent will therefore be close as well. We do not see this as a limitation, as our main goal here is not to make accurate reconstructions, but rather focus on the long-term ice volume change and the processes behind the change in glacial cycle periodicity.

The simulated MPT, and much of the glacial-interglacial variability of the past 1.5 million years results from a change in the prescribed CO_2 forcing, but the origin of the amplitude and frequency in the CO_2 record remains uncertain and was not studied here. As we use prescribed CO_2, (failed) terminations are already present in the CO_2 record: High CO_2 levels could be a symptom of successful terminations, while low CO_2 levels could be a symptom of unsuccessful terminations. Our model then replicates these failed and successful terminations. However, even with constant CO_2 levels, we can simulate many terminations during the Late Pleistocene, even though the overall periodicity does not match. A low constant CO_2 concentration (210 ppm) does skip several of these terminations. This suggest that the melt of the ice sheet could have been prompted by insolation, but it has been enhanced by an increase in CO_2. However, our simulations do not explain the ~~decrease~~change in

~~glacial~~ frequency and amplitude present in the CO_2 ~~concentrations~~record, which ~~could of course be related to~~involves ice-sheet-carbon-cycle interactions. ~~Therefore, while~~To conclude, our results suggest that CO_2 can have a key role in the MPT, and that ~~a decrease in glacial~~maintaining low CO_2 levels during insolation maxima could lengthen glacial cycles. However, to truly uncover the origin of the MPT will require a coupled ice-sheet-climate-carbon-cycle model.

5. Conclusions

In this study, we simulate the Northern Hemisphere ice sheet evolution of the past 1.5 million years using prescribed CO_2, insolation and implicit ice-sheet–climate feedbacks. Our main goal was to capture and investigate the frequency change during the MPT. We found that the modelled MPT is strongly controlled by the prescribed CO_2 levels. Before the MPT, glacial cycles are dominated by insolation, and CO_2 levels rise in phase with obliquity maximum. After the MPT, low interstadial CO_2 levels are maintained through some insolation maxima, prolonging glacial periods to an average 100 kyr.

This idea is further explored by experiments with constant insolation or CO_2. If CO_2 is constant, we can capture the frequency during the Early Pleistocene, but fail to simulate the frequency during the Late Pleistocene. Lower constant CO_2 levels can increase the length of glacial cycles, but did not generate a persistent 100-kyr periodicity. When instead forcing the model with constant insolation, we find that a small range of constant summer insolation could mostly generate the Early and/or Late Pleistocene glacial cycles. The resulting frequency spectrum of these simulations is instead dominated by the peaks in interglacial CO_2, which trigger the deglaciations.

The glacial-interglacial frequency is not only affected by CO_2 and insolation, but also by the ice volume. A small North American ice sheet will melt at relatively warm climates. A medium sized ice sheet is less sensitive as it can grow towards central Canada, where the Cordilleran and Laurentide merge, converging ice flows and ablation zones. Large ice sheets can only thicken or grow towards the warmer South, reducing growth rates. These large ice sheets can easily melt through positive melt feedbacks, such as the ice albedo, melt-elevation feedbacks and the creation of proglacial lakes

We also find that, even though the precession signal is present in the climate forcing, it is always absent in the modelled ice volume. Precession fails to initiate terminations as it generally leads to weaker integrated summer insolation maxima compared to obliquity. The modelled ice volume frequency spectrum is then dominated by successful terminations, coinciding with strong insolation maxima and thus filtering out precession.

In this study, CO_2 is used as model forcing, while in reality CO_2 is also a feedback resulting from the complex interactions in the carbon cycle. Our results show that CO_2 can play a key role in the MPT, but to unravel the mechanisms of the MPT in more detail requires a model not only with ice, climate and prescribed CO_2, but also with an explicit carbon cycle.

Appendix A: Climate forcing

The ice-sheet is forced with transient changing precipitation and temperature forcing. To reduce computational resources compared to coupled ice-climate set-ups, we interpolate between pre-calculated LGM and PI climates using a matrix method (see Berends et al., 2018; Scherrenberg et al., 2023). For the monthly ($mnth$) temperature forcing (T) at each grid-cell (x, y), we use the following linear interpolation:

$$T(x,y,mnth) = w_T(x,y)\, T_{PI}(x,y,mnth) + \left(1 - w_T(x,y)\right) T_{LGM}(x,y,mnth). \tag{A1}$$

w_T represents the interpolation weight and depends on external forcing (w_e) and an albedo feedback (w_a). We allow some extrapolation for colder than LGM or warmer than present-day climates, though each interpolation weight is capped between -0.5 and 1.5.

The external forcing interpolation weight depends on CO_2 ($CO2$; obtained from Yamamoto et al., 2022 or Bereiter et al., 2015) and caloric summer half-year insolation at 65°N ($Q_{65°N}$; Tzedakis et al., 2017). We use the following equation to calculate the weight from the prescribed forcing:

$$w_e = \frac{CO2 - 190\ \text{ppm}}{280\ \text{ppm} - 190\ \text{ppm}} + \frac{Q_{65°N} - 5.8\ GJ/m^2}{0.55\ GJ/m^2}. \tag{A2}$$

This ratio was obtained by conducting a preliminary experiment based on de Boer et al. (2013) and Berends et al. (2021b), where we modify w_e to obtain good agreement with benthic $\delta^{18}O$ from Ahn et al., (2017). We then fitted the resulting w_e to CO_2 and insolation and fine-tuned it to obtain Eq. (A2).

To calculate w_a (the albedo feedback), we first calculate 2D fields of the amount of insolation that is absorbed by the surface (I). This depends on surface albedo (α_s) and the grid-cells insolation at the top of the atmosphere (Q):

$$I(x,y) = \sum_{m=1}^{12} Q(x,y,mnth)\left(1 - \alpha_s(x,y,mnth)\right). \tag{A3}$$

The albedo is generated by the ice-sheet model. First a background albedo is applied based on the ice (0.5), land (0.2) and ocean (0.1) surfaces. We then add a layer of snow that can increase albedo to up to 0.85. Using masks, climate and insolation from PI and LGM, we calculate absorbed insolation fields for the climate time-slices as well (I_{PI} and I_{LGM}). Using these three fields, we calculate a local interpolation weight for absorbed insolation (w_i):

$$w_i(x,y) = (I(x,y) - I_{LGM}(x,y)) \,/\, (I_{PI}(x,y) - I_{LGM}(x,y))\ . \tag{A4}$$

Albedo has both a local and regional effect. We apply a gaussian smoothing of 200 km on w_i to obtain $w_{i,smooth}$. We also calculate a domain-average w_i, which is $w_{i,domain}$. These three interpolation fields are then combined to obtain the albedo feedback, following the approach by Berends et al. (2018):

$$w_a(x,y) = \frac{w_i(x,y) + 3\, w_{i,smooth}(x,y) + 3\, w_{i,domain}(x,y)}{7}. \tag{A5}$$

The albedo interpolation weight is then combined with the external forcing to obtain the w_T from Eq. (A1):

$$w_T(x,y) = \frac{3\, w_e(x,y) + w_a(x,y)}{4}. \tag{A6}$$

As such, temperature depends on CO_2, caloric summer half-year insolation and a spatially varying albedo/insolation field.

To interpolate precipitation (P), we use the following equation:

$$P = exp\begin{pmatrix}(1 - w_P(x,y))\log(P_{PI}(x,y,mnth)) \\ + w_P(x,y)\log(P_{LGM}(x,y,mnth))\end{pmatrix}. \tag{A7}$$

w_P is the interpolation weight for precipitation, and is calculated with respect to local and domain-wide topography changes, reflecting changes in atmospheric circulation and the dry climates on top of ice domes. First, we calculate the total change in topography (s) in the domain with respect to PI and LGM:

$$w_{s,domain} = \frac{\sum s - \sum s_{PI}}{\sum s_{LGM} - \sum s_{PI}} \tag{A8}$$

$w_{s,domain}$ is the interpolation weight from a domain-wide change in topography. If a grid-cell has ice during the LGM, and thus a large change in topography, we also interpolate with the local topography change:

$$w_{s,local}(x,y) = \frac{s(x,y) - s_{PI}(x,y)}{s_{LGM}(x,y) - s_{PI}(x,y)}\, w_{s,domain}(x,y). \tag{A9}$$

However, if a grid cell had ice during neither PI nor LGM, $w_{s,local}$ is equal to $w_{s,domain}$. To obtain the final interpolation weight (w_P), we combine the local and domain-wide topography change:

$$w_P(x,y) = w_{s,local}(x,y)\, w_{s,domain}(x,y). \tag{A10}$$

Appendix B: δ^{18}O model

IMAU-ICE includes a benthic δ^{18}O routine, which calculates the δ^{18}O contribution from ice volume and deep-water temperature. This method is based on de Boer et al. (2013) and Berends et al. (2021b). Deep water temperature change (ΔTd) is based on CO_2 levels ($\mathrm{CO2}$):

$$\Delta\mathrm{Td} = \left(\frac{280\ \mathrm{ppm} - \mathrm{CO2}}{280\ \mathrm{ppm} - 190\ \mathrm{ppm}}\right) 2.5°C \quad . \tag{B1}$$

A 3000 kyr running-mean is applied to reflect the lag between atmospheric and deep-ocean temperatures. We then multiply this by 0.28 to obtain the δ^{18}O contribution from deep-water temperature.

For the ice sheets, we calculate a δ^{18}O contribution for every grid-cell (I). We calculate a δ^{18}O of snow accumulation based on Clarke et al. (2005):

$$I(x,y) = I_{ref}(x,y) + 0.35(T(x,y) - T_{PI}(x,y) - \gamma(s(x,y) - s_{PI}(x,y)) - 0.0062(s(x,y) - s_{PI}(x,y)). \tag{B2}$$

Here, T represents the annual mean temperature, and s represents the surface topography. The total contribution from each ice-sheet is added together and multiplied by 1.1 to reflect that we do not simulate Antarctica. I_{ref}, which is the (present-day) reference isotope concentrations, is calculated using the following parameterization by Zwally and Giovinetto (1997):

$$I_{ref}(x,y) = 0.691 * T(x,y) - 202.172. \tag{B3}$$

We then add the deep-water and ice-sheet contributions together to obtain the benthic $\delta^{18}O$.

Code availability: The ice-sheet model IMAU-ICE is described by Berends et al. (2022). The model version used in this study, as well as configuration files are available on Zenodo [DOI will be added upon acceptation]. To conduct the simulations, additional files are required. These include the prescribed CO_2 (see Bereiter et al., 2015 and Yamamoto et al., 2022), climate forcing (PMIP4 database: https://esgf-node.ipsl.upmc.fr/search/cmip6-ipsl/, last access: 16 Aug 2024), insolation (Laskar et al., 2004, Tzedakis et al., 2017), initial topography (ETOPO: https://doi.org/10.7289/V5C8276M, Amante and Eakins, 2009; BedMachine: https://doi.org/10.5067/5XKQD5Y5V3VN, NSIDC, 2024), and basal friction (Gowan et al., 2019 and Laske and Masters, 1997). For more information, contact the corresponding author.

Data availability: The results are available in a 2 kyr (2D fields) and 100-year (scalar) output frequency at Zenodo [DOI will be added upon acceptation]. Additional 2D fields can be requested by contacting the corresponding author.

Author contributions. MS conducted the simulations and has written the manuscript. The set-up for the experiments was created by RW, CB and MS. CB provided model support. All authors have provided input to the manuscript and analysis of the results.

Competing interest. The authors declare that they have no conflict of interest.

Acknowledgements. The Dutch Research Council (NWO) Exact and Natural Sciences supported the supercomputer facilities for the Dutch National Supercomputer Snellius. We would like to acknowledge the support of SurfSara Computing and Networking Services.

Financial support. M.D.W. Scherrenberg is supported by the Netherlands Earth System Science Centre (NESSC), which is financially supported by the Ministry of Education, Culture and Science (OCW) on grant no. 024.002.001. C.J. Berends is funded by the NWO under grant no. OCENW.KLEIN.515.

References

Abe-Ouchi, A., Saito, F., Kawamura, K., Raymo, M. E., Okuno, J., Takahashi, K., and Blatter, H.: Insolation-driven 100,000-year glacial cycles and hysteresis of ice-sheet volume, Nature, 500, 190–193, https://doi.org/10.1038/nature12374, 2013.

Adkins, J. F.: The role of deep ocean circulation in setting glacial climates, Paleoceanography, 28, 539–561, https://doi.org/10.1002/palo.20046, 2013.

Ahn, S., Khider, D., Lisiecki, L. E., and Lawrence, C. E.: A probabilistic Pliocene–Pleistocene stack of benthic δ18O using a profile hidden Markov model, Dynam. Stat. Clim. Syst., 2, dzx002, https://doi.org/10.1093/climsys/dzx002, 2017.

Alder, J. R. and Hostetler, S. W.: Applying the Community Ice Sheet Model to evaluate PMIP3 LGM climatologies over the North American ice sheets, Clim. Dynam., 53, 2807–2824, https://doi.org/10.1007/s00382-019-04663-x, 2019.

Amante, C. and Eakins, B. W.: ETOPO1 1 Arc-Minute Global Relief Model: Procedures, Data Sources and Analysis. NOAA Technical Memorandum NESDIS NGDC-24, National Geophysical Data Center, NOAA [dataset], https://doi.org/10.7289/V5C8276M, 2009.

Bereiter, B., Eggleston, S., Schmitt, J., Nehrbass-Ahles, C., Stocker, T. F., Fischer, H., Kipfstuhl, S., and Chappellaz, J.: Revision of the EPICA Dome C CO2 record from 800 to 600kyr before present, Geophys. Res. Lett., 42, 542–549, https://doi.org/10.1002/2014GL061957, 2015.

Berends, C. J., de Boer, B., and van de Wal, R. S. W.: Application of HadCM3@Bristolv1.0 simulations of paleoclimate as forcing for an ice-sheet model, ANICE2.1: set-up and benchmark experiments, Geosci. Model Dev., 11, 4657–4675, https://doi.org/10.5194/gmd-11-4657-2018, 2018.

Berends, C. J., Köhler, P., Lourens, L. J., and van de Wal, R. S. W.: On the cause of the mid-Pleistocene transition, Rev. Geophys., 59, e2020RG000727, https://doi.org/10.1029/2020RG000727, 2021a.

Berends, C. J., de Boer, B., and van de Wal, R. S. W.: Reconstructing the evolution of ice sheets, sea level, and atmospheric CO_2 during the past 3.6 million years, Clim. Past, 17, 361–377, https://doi.org/10.5194/cp-17-361-2021, 2021b.

Berends, C. J., Goelzer, H., Reerink, T. J., Stap, L. B., and van de Wal, R. S. W.: Benchmarking the vertically integrated ice-sheet model IMAU-ICE (version 2.0), Geosci. Model Dev., 15, 5667– 5688, https://doi.org/10.5194/gmd-15-5667-2022, 2022.

Bintanja, R., van de Wal, R. S. W., and Oerlemans, J.: Global ice volume variations through the last glacial cycle simulated by a 3-D ice dynamical model, Quatern. Int., 95–96, 11–23, 2002.

Bintanja, R. and van de Wal, R. S. W.: North American ice-sheet dynamics and the onset of 100,000-year glacial cycles, Nature, 454, 869–872, https://doi.org/10.1038/nature07158, 2008.

Blackburn, T., Kodama, S., and Piccione, G.: Eccentricity paces late Pleistocene glaciations. Geophysical Research Letters, 51, e2024GL108751. https://doi.org/10.1029/2024GL108751, 2024.

Bouttes, N., Roche, D. M., and Paillard, D.: Impact of strong deep ocean stratification on the glacial carbon cycle, Paleoceanography, 24, Artn Pa3203 https://doi.org/10.1029/2008pa001707, 2009.

Brovkin, V., Ganopolski, A., Archer, D., Munhoven, G.: Glacial CO_2 cycle as a succession of key physical and biogeochemical processes. Clim. Past 8, 251–264. https://doi.org/10.5194/cp-8-251-2012, 2012.

Bueler, E. and Brown, J.: The shallow shelf approximation as a sliding law in a thermomechanically coupled ice sheet model, J. Geophys. Res., 114, F03008, https://doi.org/10.1029/2008JF001179, 2009.

Chalk, T. B., Hain, M. P., Foster, G. L., Rohling, E. J., Sexton, P. F., Badger, M. P. S., Cherry, S. G., Hasenfratz, A. P., Haug, G. H., Jaccard, S. L., Martínez-García, A., Palike, H., Pancost, R. D., and Wilson, P. A.: Causes of ice age intensification across the Mid-Pleistocene Transition, P. Natl. Acad. Sci. USA, 114, 13114–13119, https://doi.org/10.1073/pnas.1702143114, 2017.

Clark, P. U. and Pollard, D.: Origin of the Middle Pleistocene Transition by ice sheet erosion of regolith, Paleoceanography, 13, 1–9, https://doi.org/10.1029/97PA02660, 1998.

Clarke, G. K. C., Lhomme, N., and Marshall, S. J.: Tracer transport in the Greenland Ice Sheet – three-dimensional isotopic stratigraphy, Quaternary Sci. Rev. 24, 155–171. https://doi.org/10.1016/j.quascirev.2004.08.021, 2005.

Da, J., Zhang, Y. G., Li, G., Meng, X., Ji, J.: Low CO_2 levels of the entire Pleistocene epoch. Nat. Commun. 10, 1e9. https://doi.org/10.1038/s41467-019-12357-5, 2019.

de Boer, B., van de Wal, R. S. W., Lourens, L. J., Bintanja, R., and Reerink, T. J.: A continuous simulation of global ice volume over the past 1 million years with 3-D ice-sheet models, Clim. Dynam., 41, 1365–1384, 2013.

Detlef, H., Belt, S. T., Sosdian, S. M., Smik, L., Lear, C. H., Hall, I. R., Cabedo-Sanz, P., Husum, K., and Kender, S.: Sea ice dynamics across the Mid-Pleistocene transition in the Bering Sea, Nat. Commun., 9, 941, https://doi.org/10.1038/s41467-018-02845-5, 2018.

Dyez, K. A., Hönisch, B., and Schmidt, G. A.: Early Pleistocene Obliquity-Scale pCO2 Variability at ~1.5 Milion Years Ago, Paleoceanography and Paleoclimatology, 33, 1270–1291, https://doi.org/10.1029/2018PA003349, 2018.

Farmer, J. R., Honisch, B., Haynes, L. L., Kroon, D., Jung, S., Ford, H. L., Raymo, M. E., Jaume-Segui, M., Bell, D. B., Goldstein, S. L., Pena, L. D., Yehudai, M., and Kim, J.: Deep Atlantic Ocean carbon storage and the rise of 100,000-year glacial cycles, Nat. Geosci., 12, 355–360, https://doi.org/10.1038/s41561-019-0334-6, 2019.

Feldmann, J., Albrecht, T., Khroulev, C., Pattyn, F., and Levermann, A.: Resolution-dependent performance of grounding line motion in a shallow model compared to a full-Stokes model according to the MISMIP3d intercomparison, J. Glaciol., 60, 353–360, https://doi.org/10.3189/2014JoG13J093, 2014.

Feng, F. and Bailer-Jones, C. A. L.: Obliquity and precession as pacemakers of Pleistocene deglaciations. Quat. Sci. Rev. 122, 166e179, https://doi.org/10.1016/ j.quascirev.2015.05.006, 2015.

Fettweis, X., Hofer, S., Krebs-Kanzow, U., Amory, C., Aoki, T., Berends, C. J., Born, A., Box, J. E., Delhasse, A., Fujita, K., Gierz, P., Goelzer, H., Hanna, E., Hashimoto, A., Huybrechts, P., Kapsch, M.-L., King, M. D., Kittel, C., Lang, C., Langen, P. L., Lenaerts, J. T. M., Liston, G. E., Lohmann, G., Mernild, S. H., Mikolajewicz, U., Modali, K., Mottram, R. H., Niwano, M., Noël, B. P. Y., Ryan, J. C., Smith, A., Streffing, J., Tedesco, M., van de Berg, W. J., van den Broeke, M. R., van de Wal, R. S. W., van Kampenhout, L., Wilton, D., Wouters, B., Ziemen, F., and Zolles, T.: GrSMBMIP: intercomparison of the modelled 1980-2012 surface mass balance over the Greenland Ice Sheet, The Cryosphere 14, 3935-3958, https://doi.org/10.5194/tc-14-3935-2020, 2020.

Ganopolski, A. and Calov, R.: The role of orbital forcing, carbon dioxide and regolith in 100 kyr glacial cycles, Clim. Past, 7, 1415–1425, https://doi.org/10.5194/cp-7-1415-2011, 2011.

Gomez, N., Gregoire, L., Mitrovica, J., and Payne, A.: Laurentide-Cordilleran Ice Sheet saddle collapse as a contribution to meltwater pulse 1A, Geophys. Res. Lett., 42, 3954–3962, https://doi.org/10.1002/2015GL063960, 2015.

Gowan, E. J., Niu, L., Knorr, G., and Lohmann, G.: Geology datasets in North America, Greenland and surrounding areas for use with ice sheet models, Earth Syst. Sci. Data, 11, 375–391, https://doi.org/10.5194/essd-11-375-2019, 2019.

Hasenfratz, A. P., Jaccard, S. L., Martínez-García, A., Sigman, D. M., Hodell, D. A., Vance, D., Bernasconi, S. M., Kleiven, H. F., Haumann, F. A., and Haug, G. H.: The residence time of Southern Ocean surface waters and the 100 000-year ice age cycle, Science, 363, 1080–1084, https://doi.org/10.1126/science.aat7067, 2019.

Hinck, S., Gowan, E. J., Zhang, X., and Lohmann, G.: PISM-LakeCC: Implementing an adaptive proglacial lake boundary in an ice sheet model, The Cryosphere, 16, 941–965, https://doi.org/10.5194/tc-16-941-2022, 2022.

Hobart, B., Lisiecki, L. E., Rand, D., Lee, T., and Lawrence, C. E.: Late Pleistocene 100-kyr glacial cycles paced by precession forcing of summer insolation, Nat. Geosci., 16, 717–722, https://doi.org/10.1038/s41561-023-01235-x, 2023.

Hönisch, B., Hemming, N.G., Archer, D., Siddall, M., McManus, J.F.: Atmospheric carbon dioxide concentration across the mid-Pleistocene transition. Science 324, 1551–1554, https://doi.org/10.1126/science.1171477, 2009.

Huybers, P. and Wunsch, C.: Obliquity pacing of the late Pleistocene glacial terminations, Nature, 434, 491–494, 2005.

Huybers, P.: Early Pleistocene glacial cycles and the integrated summer insolation forcing, Science, 313, 508–511, https://doi.org/10.1126/science.1125249, 2006.

Huybers, P. and Tziperman, E.: Integrated summer insolation forcing and 40,000-year glacial cycles: The perspective from an ice-sheet/energy-balance model, Paleoceanography, 23, https://doi.org/10.1029/2007PA001463, 2008.

Huybers, P.: Combined obliquity and precession pacing of late Pleistocene deglaciations, Nature, 480, 229–232, https://doi.org/10.1038/nature10626, 2011.

Huybrechts, P. and de Wolde, J.: The dynamic response of the Greenland and Antarctic ice sheets to multiple-century climatic warming, J. Climate 1, 2169–2188, 1999.

Kageyama, M., Albani, S., Braconnot, P., Harrison, S. P., Hopcroft, P. O., Ivanovic, R. F., Lambert, F., Marti, O., Peltier, W. R., Peterschmitt, J.-Y., Roche, D. M., Tarasov, L., Zhang, X., Brady, E. C., Haywood, A. M., LeGrande, A. N., Lunt, D. J., Mahowald, N. M., Mikolajewicz, U., Nisancioglu, K. H., Otto-Bliesner, B. L., Renssen, H., Tomas, R. A., Zhang, Q., Abe-Ouchi, A., Bartlein, P. J., Cao, J., Li, Q., Lohmann, G., Ohgaito, R., Shi, X., Volodin, E., Yoshida, K., Zhang, X., Zheng, W.: The PMIP4 contribution to CMIP6 – Part 4: Scientific objectives and experimental design of the PMIP4-CMIP6 Last Glacial Maximum experiments and PMIP4 sensitivity experiments, Geosci. Model Dev., 10, 4035–4055, https://doi.org/10.5194/gmd-10-4035-2017, 2017.

Kageyama, M., Braconnot, P., Harrison, S. P., Haywood, A. M., Jungclaus, J. H., Otto-Bliesner, B. L., Peterschmitt, J.-Y., Abe- Ouchi, A., Albani, S., Bartlein, P. J., Brierley, C., Crucifix, M., Dolan, A., Fernandez-Donado, L., Fischer, H., Hopcroft, P. O., Ivanovic, R. F., Lambert, F., Lunt, D. J., Mahowald, N. M., Peltier, W. R., Phipps, S. J., Roche, D. M., Schmidt, G. A., Tarasov, L., Valdes, P. J., Zhang, Q., Zhou, T.: The PMIP4 contribution to CMIP6 – Part 1: Overview and overarching analysis plan, Geosci. Model Dev. 11, 1033–1057, https://doi.org/10.5194/gmd-11-1033-2018, 2018

Kageyama, M., Harrison, S. P., Kapsch, M.-L., Löfverström, M., Lora, J. M., Mikolajewicz, U., Sherriff-Tadano, S., Vadsaria, T., Abe-Ouchi, A., Bouttes, N., Chandan, D., Gregoire, L. J., Ivanovic, R. F., Izumi, K., LeGrande, A. N., Lhardy, F., Lohmann, G., Morozova, P. A., Ohgaito, R., Paul, A., Peltier, W. R., Poulsen, C. J., Quiquet, A., Roche, D. M., Shi, X., Tierney, J. E., Valdes, P. J., Volodin, E., and Zhu, J.: The PMIP4 Last Glacial Maximum experiments: preliminary results and comparison with the PMIP3 simulations, Clim. Past, 17, 1065–1089, https://doi.org/10.5194/cp-17-1065-2021, 2021.

Köhler, P. and Bintanja, R.: The carbon cycle during the Mid Pleistocene Transition: the Southern Ocean Decoupling Hypothesis, Clim. Past, 4, 311–332, https://doi.org/10.5194/cp-4-311-2008, 2008.

Kurahashi-Nakamura, T., Abe-Ouchi, A., and Yamanaka, Y.: Effects of physical changes in the ocean on the atmospheric pCO2: glacial-interglacial cycles, Clim. Dynam., 35, 713–719, https://doi.org/10.1007/s00382-009-0609-5, 2010.

Laskar, J., Robutel, P., Joutel, F., Gastineau, M., Correia, A. C. M., and Levrard, B.: A long-term numerical solution for the insolation quantities of the Earth, Astron. Astrophys., 428, 261–285, https://doi.org/10.1051/0004-6361:20041335, 2004.

Laske, G. and Masters, G.: A Global Digital Map of Sediment Thickness, EOS T. Am. Geophys. Un., 78, F483, 1997.

Lear, C. H., Billups, K., Rickaby, R. E. M., Diester-Haass, L., Mawbey, E. M., and Sosdian, S. M.: Breathing more deeply: Deep ocean carbon storage during the mid-Pleistocene climate transition, Geology, 44, 1035–1038, https://doi.org/10.1130/G38636.1, 2016.

Legrain, E., Parrenin, F., and Capron, E.: A gradual change is more likely to have caused the Mid-Pleistocene Transition than an abrupt event, Commun. Earth Environ., 4, 1–10, https://doi.org/10.1038/s43247-023-00754-0, 2023.

Leguy, G. R., Lipscomb, W. H., and Asay-Davis, X. S.: Marine ice sheet experiments with the Community Ice Sheet Model, The Cryosphere, 15, 3229–3253, https://doi.org/10.5194/tc-15-3229- 2021, 2021.

Le Meur, E. and Huybrechts, P.: A comparison of different ways of dealing with isostasy: examples from modeling the Antarctic ice sheet during the last glacial cycle, Ann. Glaciol., 23, 309–317, https://doi.org/10.3189/S0260305500013586, 1996.

Lisiecki, L. E.: Links between eccentricity forcing and the 100,000-year glacial cycle, Nat. Geosci., 3, 349–352, https://doi.org/10.1038/ngeo828, 2010.

Martin, J. H.: Glacial-interglacial CO2 change: the iron hypothesis, Paleoceanography, 5, 1–13, https://doi.org/10.1029/PA005i001p00001, 1990.

Martin, M. A., Winkelmann, R., Haseloff, M., Albrecht, T., Bueler, E., Khroulev, C., and Levermann, A.: The Potsdam Parallel Ice Sheet Model (PISM-PIK) – Part 2: Dynamic equilibrium simulation of the Antarctic ice sheet, The Cryosphere, 5, 727–740, https://doi.org/10.5194/tc-5-727-2011, 2011.

Martínez-García, A., Sigman, D. M., Ren, H., Anderson, R., Straub, M., Hodell, D., Jaccard, S., Eglinton, T. I., and Haug, G. H.: Iron fertilization of the subantarctic ocean during the last ice age, Science, 343, 1347–1350, https://doi.org/10.1126/science.1246848, 2014.

Mauritsen, T., Bader, J., Becker, T., Behrens, J., Bittner, M., Brokopf, R., Brovkin, V., Claussen, M., Crueger, T., Esch, M., Fast, I., Fiedler, S., Fläschner, D., Gayler, V., Giorgetta, M., Goll, D. S., Haak, H., Hagemann, S., Hedemann, C., Hohenegger, C., Ilyina, T., Jahns, T., Jimenéz-de-la Cuesta, D., Jungclaus, J., Kleinen, T., Kloster, S., Kracher, D., Kinne, S., Kleberg, D., Lasslop, G., Kornblueh, L., Marotzke, J., Matei, D., Meraner, K., Mikolajewicz, U., Modali, K., Möbis, B., Müller, W. A., Nabel, J. E., Nam, C. C., Notz, D., Nyawira, S. S., Paulsen, H., Peters, K., Pincus, R., Pohlmann, H., Pongratz, J., Popp, M., Raddatz, T. J., Rast, S., Redler, R., Reick, C. H., Rohrschneider, T., Schemann, V., Schmidt, H., Schnur, R., Schulzweida, U., Six, K. D., Stein, L., Stemmler, I., Stevens, B., von Storch, J. S., Tian, F., Voigt, A., Vrese, P., Wieners, K. H., Wilkenskjeld, S., Winkler, A., and Roeckner, E.: Developments in the MPI-M Earth System Model version 1.2 (MPI-ESM1.2) and Its Response to Increasing CO_2, Journal of Advances in Modeling Earth Systems 11, 998–1038, https://doi.org/10.1029/2018MS001400, 2019.

Menviel, L. (2019). The southern amplifier. Science, 363, 1040–1041. https://doi.org/10.1126/science.aaw7196

Mitsui, T., Willeit, M., Boers, N.: Synchronization phenomena observed in glacial–interglacial cycles simulated in an Earth system model of intermediate complexity, Earth Syst. Dynam. 14, 1277–1294, https://doi.org/10.5194/esd-14-1277-2023, 2023.

Niu, L., Lohmann, G., Hinck, S., Gowan, E. J., and Krebs-Kanzow, U.: The sensitivity of Northern Hemisphere ice sheets to atmospheric forcing during the last glacial cycle using PMIP3 models, J. Glaciol., 65, 645–661, https://doi.org/10.1017/jog.2019.42, 2019.

NSIDC: IceBridge BedMachine Greenland, Version 1, NSICDC [data set], https://doi.org/10.5067/5XKQD5Y5V3VN, 2024.

Ohgaito, R., Yamamoto, A., Hajima, T., O'ishi, R., Abe, M., Tatebe, H., Abe-Ouchi, A., Kawamiya, M.: PMIP4 experiments using MIROC-ES2L Earth system model, Geosci. Model Dev. 14, 1195–1217, https://doi.org/10.5194/gmd-14-1195-2021, 2021.

Ohmura, A., Calanca, P., Wild, M. and Anklin M.: Precipitation, accumulation and mass balance of the Greenland Ice sheet, Z. Gletscherkd. Glazialgeol., 35(1), 1–20, 1999.

Paillard, D.: The timing of Pleistocene glaciations from a simple multiple-state climate model, Nature, 391, 378–381, https://doi.org/10.1038/34891, 1998.

Parrenin, F. and Paillard, D.: Amplitude and phase of glacial cycles from a conceptual model, Earth Planet. Sc. Lett., 214, 243–250, 2003.

Peltier, W. R., Argus, D. F., and Drummond, R.: Space geodesy constrains ice age terminal deglaciation: The global ICE6G_C(VM5a) model, J. Geophys. Res.-Solid, 120, 450–487, https://doi.org/10.1002/2014JB011176, 2015.

Pena, L. D. and Goldstein, S. L.: Thermohaline circulation crisis and impacts during the mid-Pleistocene transition, Science, 345, 318–322, https://doi.org/10.1126/science.1249770, 2014.

Portier, A. M., Thierens, M., Martin, E. E., Hemming, S. R., Gombiner, J. H., and Raymo, M. E.: Late Pleistocene emergence of crystalline Canadian Shield sources in sediments of the northern Gulf of Mexico, Paleoceanography and Paleoclimatology 36, e2020PA004082, https://doi. org/10.1029/2020PA004082, 2021.

Qin, B., Jia, Q., Xiong, Z., Li, T., Algeo, T. J. and Dang, H.: Sustained Deep Pacific carbon storage after the Mid-Pleistocene Transition linked to enhanced Southern Ocean stratification, Geophys. Res. Lett. 49, e2021GL097121, https://doi.org/10.1029 /2021GL097121, 2022.

Quiquet, A., Dumas, C., Paillard, D., Ramstein, G., Ritz, C., and Roche, D. M.: Deglacial Ice Sheet Instabilities Induced by Proglacial Lakes, Geophys. Res. Lett., 48, e2020GL092141, https://doi.org/10.1029/2020GL092141, 2021.

Roe, G. H. and Lindzen, R. S.: The Mutual Interaction between Continental-Scale Ice Sheets and Atmospheric Stationary Waves, J. Climate, 14, 1450–1465, 2001.

Rohling, E. J., Yu, J., Heslop, D., Foster, G. L., Opdyke, B., and Roberts, A. P.: Sea level and deep-sea temperature reconstructions suggest quasi-stable states and critical transitions over the past 40 million years, Science Advances, 7, eabf5326, https://doi.org/10.1126/sciadv.abf5326, 2021

Roy, M., Clark, P. U., Raisbeck, G. M., and Yiou, F.: Geochemical constraints on the regolith hypothesis for the middle Pleistocene transition, Earth and Planetary Science Letters, 227, 281–296, https://doi.org/10.1016/j.epsl.2004.09.001, 2004.

Saini, H., Meissner, K. J., Menviel, L., and Kvale, K.: Impact of iron fertilisation on atmospheric CO_2 during the last glaciation, Clim. Past, 19, 1559–1584, https://doi.org/10.5194/cp-19-1559-2023, 2023.

Scherrenberg, M. D. W., Berends, C. J., Stap, L. B., and van de Wal, R. S. W.: Modelling feedbacks between the Northern Hemisphere ice sheets and climate during the last glacial cycle, Clim. Past, 19, 399–418, https://doi.org/10.5194/cp-19-399-2023, 2023.

Scherrenberg, M. D. W., Berends, C. J., and van de Wal, R. S. W.: Late Pleistocene glacial terminations accelerated by proglacial lakes, Clim. Past, 20, 1761–1784, https://doi.org/10.5194/cp-20-1761-2024, 2024.

Shi, X., Werner, M., Yang, H., D'Agostino, R., Liu, J., Yang, C., Lohmann, G.: Unraveling the complexities of the Last Glacial Maximum climate: the role of individual boundary conditions and forcings, Clim. Past 19, 2157–2175, https://doi.org/10.5194/cp-19-2157-2023, 2023.

Sigman, D. M., Boyle, E. A.: Glacial/interglacial variations in atmospheric carbon dioxide. Nature, 407, 859–869. https://doi.org/10.1038/35038000, 2000

Sigman, D. M., Hain, M. P., Haug, G. H.: The polar ocean and glacial cycles in atmospheric CO_2 concentration. Nature, 466, 47–55. https://doi.org/10.1038/nature09149, 2010

Spratt, R. M. and Lisiecki, L. E.: A Late Pleistocene sea level stack, Clim. Past, 12, 1079–1092, https://doi.org/10.5194/cp-12-1079-2016, 2016.

Tabor, C. R., Poulsen, C. J., and Pollard, D.: How obliquity cycles powered early Pleistocene global ice-volume variability, Geophys. Res. Lett., 42, 1871–1879, https://doi.org/10.1002/2015GL063322, 2015.

Tabor, C. R. and Poulsen, C. J.: Simulating the mid-Pleistocene transition through regolith removal, Earth Planet. Sc. Let., 434, 231–240, https://doi.org/10.1016/j.epsl.2015.11.034, 2016.

Thomas, N. C., Bradbury, H. J., Hodell, D. A., 2022. Changes in North Atlantic deep-water oxygenation across the Middle Pleistocene Transition. Science 377, 654–659, https://doi.org/10.1126/science.abj7761

Tzedakis, P. C., Crucifix, M., Mitsui, T., and Wolff, E. W.: A simple rule to determine which insolation cycles lead to interglacials, Nature, 542, 427–432, https://doi.org/10.1038/nature21364, 2017.

Verbitsky, M. Y., Crucifix, M., and Volobuev, D. M.: A theory of Pleistocene glacial rhythmicity, Earth Syst. Dynam., 9, 1025–1043, https://doi.org/10.5194/esd-9-1025-2018, 2018.

Volodin, E. M., Mortikov, E. V., Kostrykin, S. V., Galin, V. Y., Lykossov, V. N., Gritsun, A. S., Diansky, N. A., Gusev, A. V., Iakovlev, N. G., Shestakova, A. A., and Emelina, S. V.: Simulation of the modern climate using the INM-CM48 climate model. Russ. J. Numer. Anal. M 33, 367–374. https://doi.org/10.1515/rnam-2018-0032, 2018

Watanabe, Y., Abe-Ouchi, A., Saito, F., Kino, K., O'ishi, R., Ito, T., Kawamura, K., and Chan, W.-L.: Astronomical forcing shaped the timing of early Pleistocene glacial cycles, Communications Earth & Environment, 4, 2023.

Willeit, M., Ganopolski, A., Calov, R., and Brovkin, V.: Mid-Pleistocene transition in glacial cycles explained by declining CO_2 and regolith removal, Sci. Adv., 5, eaav7337, https://doi.org/10.1126/sciadv.aav7337, 2019.

Yamamoto, M., Clemens, S. C., Seki, O., Tsuchiya, Y., Huang, Y., O'ishi, R., and Abe-Ouchi, A.: Increased interglacial atmospheric CO_2 levels followed the mid-Pleistocene Transition, Nat. Geosci., 15, 307–313, https://doi.org/10.1038/s41561-022-00918-1 2022.

Zwally, H. J. and Giovinetto, M. B.: Areal distribution of the oxygen-isotope ratio in Greenland, Ann. Glaciol., 25, 208–213, https://doi.org/10.3189/S0260305500014051, 1997.